AD 740828

MICROSTRUCTURE STUDIES OF REFRACTORY POLYCRYSTALLINE OXIDES

SUMMARY REPORT

9 March 1971 to 9 January 1972

Contract N00019-71-C-0325

Prepared for

U.S. Naval Air Systems
Washington, D.C.

Prepared by

W.H. Rhodes
P.L. Berneburg
R.M. Cannon

AVCO CORPORATION
Systems Division
Lowell, Massachusetts 01851

93

Unclassified

Security Classification

DOCUMENT CONTROL DATA - R&D

(Security classification of title, body of abstract and indexing annotation must be entered when the overall report is classified)

1. ORIGINATING ACTIVITY (Corporate author)

Avco Corporation
Systems Division
Lowell, Massachusetts 01851

2a. REPORT SECURITY CLASSIFICATION

Unclassified

2b. GROUP

3. REPORT TITLE

Microstructure Studies of Refractory Polycrystalline Oxides

4. DESCRIPTIVE NOTES (Type of report and inclusive dates)

Summary Report, 9 March 1971 to 9 January 1972

5. AUTHOR(S) (Last name, first name, initial)

Rhodes, William H.
Berneburg, Philip L.
Cannon, Rowland M.

6. REPORT DATE	7a. TOTAL NO. OF PAGES	7b. NO. OF REFS
9 March 1971 to 9 January 1972	62	20

8a. CONTRACT OR GRANT NO.	9a. ORIGINATOR'S REPORT NUMBER(S)
N00019-71-C-0325	
b. PROJECT NO.	
c.	9b. OTHER REPORT NO(S) (Any other numbers that may be assigned this report)
d.	

10. AVAILABILITY/LIMITATION NOTICES

Approved for public release: unlimited distribution

11. SUPPLEMENTARY NOTES	12. SPONSORING MILITARY ACTIVITY
	Naval Air Systems Command Washington, D.C.

13. ABSTRACT

This program was divided into three tasks within the general topic of microstructure effects on properties of polycrystalline oxides. The first task was concerned with the identification, origin, and elimination of strength limiting flaws in fine grained high density hot pressed alumina. Careful examination of transverse bend bars fracture surfaces from four billets made with two different powders and two basically different process cycles, revealed material flaw fracture origins in 60% of the bars, surface scratch flaw origins in 12% of the bars, and no detectable fracture origin in 28% of the bars. The principal strength limiting material flaws were either defects traceable to chemical contamination or large grains grown by exaggerated growth. These defects were studied in detail and in a number of cases the source of the defect was identified. The discussion also dealt with the implications of these findings on the various brittle fracture theories.

The fabrication of complex alumina shapes by the press forging process was studied with a goal of achieving not only the prescribed shape, but the unique optical and mechanical properties of press forged alumina. Pre-sintered right circular preforms were forged into thin shell hemispheres with 60% in-line transmission at 2 mm thickness and 5 um wavelength. Strain rate control was shown to be very critical and an effective deformation schedule was defined.

The consolidation of high purity fine particulate organo-metallic derived Al_2O_3 was studied on a cooperative program with the Air Force Materials Laboratory. Specimens in excess of 99% density with a 4 um grain size were fabricated.

cont.

DD FORM 1 JAN 64 1473

Unclassified

Security Classification

Unclassified

Security Classification

14. KEY WORDS	LINK A ROLE	LINK A WT	LINK B ROLE	LINK B WT	LINK C ROLE	LINK C WT
Alumina						
Magnesia						
Hot Pressing						
Press Forging						
Mechanical Properties						
High Purity						
Brittle Fracture						
Defect Analysis						

INSTRUCTIONS

1. ORIGINATING ACTIVITY: Enter the name and address of the contractor, subcontractor, grantee, Department of Defense activity or other organization *(corporate author)* issuing the report.

2a. REPORT SECURITY CLASSIFICATION: Enter the overall security classification of the report. Indicate whether "Restricted Data" is included. Marking is to be in accordance with appropriate security regulations.

2b. GROUP: Automatic downgrading is specified in DoD Directive 5200.10 and Armed Forces Industrial Manual. Enter the group number. Also, when applicable, show that optional markings have been used for Group 3 and Group 4 as authorized.

3. REPORT TITLE: Enter the complete report title in all capital letters. Titles in all cases should be unclassified. If a meaningful title cannot be selected without classification, show title classification in all capitals in parenthesis immediately following the title.

4. DESCRIPTIVE NOTES: If appropriate, enter the type of report, e.g., interim, progress, summary, annual, or final. Give the inclusive dates when a specific reporting period is covered.

5. AUTHOR(S): Enter the name(s) of author(s) as shown on or in the report. Enter last name, first name, middle initial. If military, show rank and branch of service. The name of the principal author is an absolute minimum requirement.

6. REPORT DATE: Enter the date of the report as day, month, year; or month, year. If more than one date appears on the report, use date of publication.

7a. TOTAL NUMBER OF PAGES: The total page count should follow normal pagination procedures, i.e., enter the number of pages containing information.

7b. NUMBER OF REFERENCES: Enter the total number of references cited in the report.

8a. CONTRACT OR GRANT NUMBER: If appropriate, enter the applicable number of the contract or grant under which the report was written.

8b, 8c, & 8d. PROJECT NUMBER: Enter the appropriate military department identification, such as project number, subproject number, system numbers, task number, etc.

9a. ORIGINATOR'S REPORT NUMBER(S): Enter the official report number by which the document will be identified and controlled by the originating activity. This number must be unique to this report.

9b. OTHER REPORT NUMBER(S): If the report has been assigned any other report numbers *(either by the originator or by the sponsor)*, also enter this number(s).

10. AVAILABILITY/LIMITATION NOTICES: Enter any limitations on further dissemination of the report, other than those imposed by security classification, using standard statements such as:

(1) "Qualified requesters may obtain copies of this report from DDC."

(2) "Foreign announcement and dissemination of this report by DDC is not authorized."

(3) "U. S. Government agencies may obtain copies of this report directly from DDC. Other qualified DDC users shall request through

________________________________."

(4) "U. S. military agencies may obtain copies of this report directly from DDC. Other qualified users shall request through

________________________________."

(5) "All distribution of this report is controlled. Qualified DDC users shall request through

________________________________."

If the report has been furnished to the Office of Technical Services, Department of Commerce, for sale to the public, indicate this fact and enter the price, if known.

11. SUPPLEMENTARY NOTES: Use for additional explanatory notes.

12. SPONSORING MILITARY ACTIVITY: Enter the name of the departmental project office or laboratory sponsoring *(paying for)* the research and development. Include address.

13. ABSTRACT: Enter an abstract giving a brief and factual summary of the document indicative of the report, even though it may also appear elsewhere in the body of the technical report. If additional space is required, a continuation sheet shall be attached.

It is highly desirable that the abstract of classified reports be unclassified. Each paragraph of the abstract shall end with an indication of the military security classification of the information in the paragraph, represented as *(TS)*, *(S)*, *(C)*, or *(U)*.

There is no limitation on the length of the abstract. However, the suggested length is from 150 to 225 words.

14. KEY WORDS: Key words are technically meaningful terms or short phrases that characterize a report and may be used as index entries for cataloging the report. Key words must be selected so that no security classification is required. Identifiers, such as equipment model designation, trade name, military project code name, geographic location, may be used as key words but will be followed by an indication of technical context. The assignment of links, rules, and weights is optional.

Unclassified

Security Classification

cont.

Unclassified

Security Classification

DOCUMENT CONTROL DATA - R & D

(Security classification of title, body of abstract and indexing annotation must be entered when the overall report is classified)

1. ORIGINATING ACTIVITY (Corporate author) Avco Corporation Systems Division Lowell, Massachusetts 01851	2a. REPORT SECURITY CLASSIFICATION Unclassified 2b. GROUP

3. REPORT TITLE

Microstructure Studies of Refractory Polycrystalline Oxides

4. DESCRIPTIVE NOTES (Type of report and inclusive dates)
Summary Report, 9 March 1971 to 9 January 1972

5. AUTHOR(S) (First name, middle initial, last name)
Rhodes, William H.
Berneburg, Philip L.
Cannon, Rowland M.

6. REPORT DATE 9 March 1971 to 9 January 1972	7a. TOTAL NO. OF PAGES 62	7b. NO. OF REFS 20
8a. CONTRACT OR GRANT NO. N00019-71-C-0325 b. PROJECT NO. c. d.	9a. ORIGINATOR'S REPORT NUMBER(S) 9b. OTHER REPORT NO(S) (Any other numbers that may be assigned this report)	

10. DISTRIBUTION STATEMENT

11. SUPPLEMENTARY NOTES	12. SPONSORING MILITARY ACTIVITY Naval Air Systems Command Washington, D.C.

13. ABSTRACT

cont.

Intra-agglomerate densification was identified as a possible rate and microstructure limiting process. Various powder preparation processes were identified and judged worthy of continued research.

DD FORM 1 NOV 65 1473

UNCLASSIFIED

Security Classification

MICROSTRUCTURE STUDIES OF REFRACTORY POLYCRYSTALLINE OXIDES

SUMMARY REPORT

9 March 1971 to 9 January 1972

Contract N00019-71-C-0325

Prepared for

U.S. Naval Air Systems
Washington, D.C.

Approved by

T. Vasilos

T. Vasilos

Prepared by

W.H. Rhodes
P.L. Berneburg
R.M. Cannon

AVCO CORPORATION
Systems Division
Lowell, Massachusetts 01851

A)proved for Public Release: Distribution Unlimited.

FOREWORD

This report was prepared by the Systems Division of Avco Corporation under U.S. Navy Contract N00019-71-C-0325 entitled, Microstructure Studies of Polycrystalline Oxides.

The work was administered under the direction of the U.S. Department of the Navy, Air Systems Command, with Mr. Charles F. Bersch, Code AIR-52032A, acting as Project Engineer.

This report covers work conducted from 9 March 1971 to 9 January 1972.

The writers are pleased to acknowledge the contributions of the following individuals to this program; B. MacAllister for mechanical evaluation, R. Gardner for ceramographic preparation, J. Centorino and E. Vallante for materials preparation, C.L. Houck for electron microscopy, and T. Vasilos and J. Niesse for useful discussions.

ABSTRACT

This program was divided into three tasks within the general topic of microstructure effects on properties of polycrystalline oxides. The first task was concerned with the identification, origin, and elimination of strength limiting flaws in fine grained, high density, hot pressed alumina. Careful examination of transverse bend bars fracture surfaces from four billets made with two different powders and two basically different process cycles, revealed material flaw fracture origins in 60% of the bars, surface scratch flaw origins in 12% of the bars, and no detectable fracture origin in 28% of the bars. The principal strength limiting material flaws were either defects traceable to chemical contamination or large grains grown by exaggerated growth. These defects were studied in detail and in a number of cases the source of the defect was identified. The discussion also dealt with the implications of these findings on the various brittle fracture theories.

The fabrication of complex alumina shapes by the press forging process was studied with a goal of achieving not only the prescribed shape, but the unique optical and mechanical properties of press forged alumina. Presintered right circular preforms were forged into thin shell hemispheres with 60% in-line transmission at 2 mm thickness and 5 µm wavelength. Strain rate control was shown to be very critical and an effective deformation schedule was defined.

The consolidation of high purity fine particulate organo-metallic derived Al_2O_3 was studied on a cooperative program with the Air Force Materials Laboratory. Specimens in excess of 99% density with a 4 µm grain size were fabricated. Intra-agglomerate densification was identified as a possible rate and microstructure limiting process. Various powder preparation processes were identified and judged worthy of continued research.

TABLE OF CONTENTS

LIST OF FIGURES

LIST OF FIGURES cont.

LIST OF TABLES

I. INTRODUCTION

This program was divided into three tasks within the very broad topic of microstructure effects on properties of polycrystalline oxides. The first area to be described deals with the cause and effect of strength limiting flaws in fine grained dense hot pressed Al_2O_3. This is appropriate as designers need ceramics with more consistent mechanical properties. If strengths could be raised, this would be a side and well received benefit, but a low standard deviation around a 70,000 psi strength would be of considerable value from a design viewpoint. It was also thought that this study would influence the current controversy between Griffith crack and dislocation nucleated fracture in polycrystalline Al_2O_3 at room temperature.

The second area of study is a continuation of press forging process research. Earlier work had demonstrated the unique optical and mechanical properties of press forged Al_2O_3. It was also shown that this technique could be used to form a thin shell hemisphere from a circular right cylinder preform, thus establishing a new technology for the forming of shaped ceramics. The objective of this study was to continue process research aiming toward the achievement of a hemisphere with equivalent properties to those observed for flat plate forgings.

The final area to be discussed is the consolidation of alkoxy derived high purity Al_2O_3. This study is being conducted as a joint project with Mr. K.S. Mazdiyasni of the Air Force Materials Laboratory. The goal of this study is the achievement of a fine grained ultra high purity polycrystalline Al_2O_3 body which would aid in the separation of structure sensitive and composition sensitive mechanical behavior. If unique properties were obtained, this would be of interest from an application viewpoint.

II. FLAWS IN ALUMINA AND EFFECT ON STRENGTH

A. General

The Weibull theory of flaw distribution has been shown[1] to be applicable to the description of brittle strength in hot pressed Al_2O_3. It is thought that at least two types of flaws are responsible for fracture. Fractures outside the gage length of a bend test or the low values of the strength distribution curve are probably caused by large flaws that are chemically and/or structurally different from the matrix (designated Type I flaws). The second type of flaw is responsible for the fracture at the average and high end of the strength distribution curve in a material that has a low enough concentration of Type I flaws that all of the fractures are not related to Type I flaws. These Type II flaws are probably associated with the normal microstructural features usually considered as intrinsic. It is the Type I flaw that must initially be found, characterized, identified, and eliminated if Al_2O_3 is to be utilized structurally near its mean strength (questions of corrosion and fatigue are important also). This type of flaw should be apparent during the course of ambient atmosphere bend tests. Careful microscopic flaw analysis of fracture specimens was the approach taken for this study. It is expected ultimately that work can also be accomplished in the area of inherent flaw analysis, although this study will be directed toward Type I flaws.

B. Powder Characterization

Powder selected for this program was supplied by a vendor previously used for many fabrication studies on moderately high purity Al_2O_3 with a specification of 99.98% pure and 0.3 micron particle size. Emission or mass spectrographic analysis of starting powders gives a very selective volume analysis which may or may not be representative of the total batch. Further, an impurity particle or high concentration of solid solution impurities could be completely by-passed in the sample selection process. Therefore, Vendor I powder lots 106 and 119 were subjected to a screening, culling, and x-ray analysis in addition to the standard emission spectrographic analysis.

The powders were screened through 200 mesh (74 micron) screen. Examination of the +200 mesh fraction under a stereomicroscope revealed foreign particulates consisting of non-oxide looking material and apparent oxides with non-alumina morphologies. In the first category were organic-looking fibers (probably cellulose), metal turnings, yellow-brown flakes, shiny black flakes resembling graphite, and black grains, and miscellaneous particles of various colors (green, pink, red) all of which are illustrated in Figure 1. In the second category were numerous colorless, transparent to translucent particles, and red-brown particles (possibly α-Fe_2O_3). All such particles which could be found in the +200 fraction of lot 106 were removed and, under a polarizing microscope, separated into anisotropic and isotropic fractions. Debye-Scherrer analysis showed the anisotropic fraction, as illustrated in Figure 2, to be single crystal alpha quartz grains and the isotropic fraction to be polycrystalline alpha cristobalite particles. The apparent optical isotropy of the cristobalite particles was probably due to fine polycrystallinity. The anisotropic and isotropic fractions both showed one additional unidentified phase which may be a phosphate such as $Na_4P_2O_7 \cdot 10\,H_2O$. The diffraction patterns of this latter phase were similar to unidentified reflections obtained from the small spherical defects found in a hot pressed billet.

In addition to the obviously foreign particles, the +200 fraction from lot 106 showed three different Al_2O_3 particle morphologies: predominant irregular, opaque white particles and flakes, as well as opaque white spherical particles (approximately 0.1 mm diameter), and translucent bluish-white flakes. Debye-Scherrer analysis showed all three to be primarily α-Al_2O_3 with minor amounts of a poorly crystalline transition Al_2O_3. The bluish-white flakes appeared to contain more of the transition form than the other two types.

Semi-quantitative emission spectrographic impurity analyses for these two powder lots and a third lot used in this phase of the program are reported in Table I. Judging by these analyses, the overall impurity concentrations were extremely low, giving the impression that the powders were of high quality. It is now thought that these analyses do not adequately represent the gross particulate impurities discussed above.

Although powder from only one vendor was subjected to this detailed analysis, the authors believe that other suppliers of Al_2O_3 powder marketed under a similar specification are subject to similar findings. This will

5482-4B 15X

Figure 1. Non-Ceramic Inclusions Separated from Powder Lot 119.

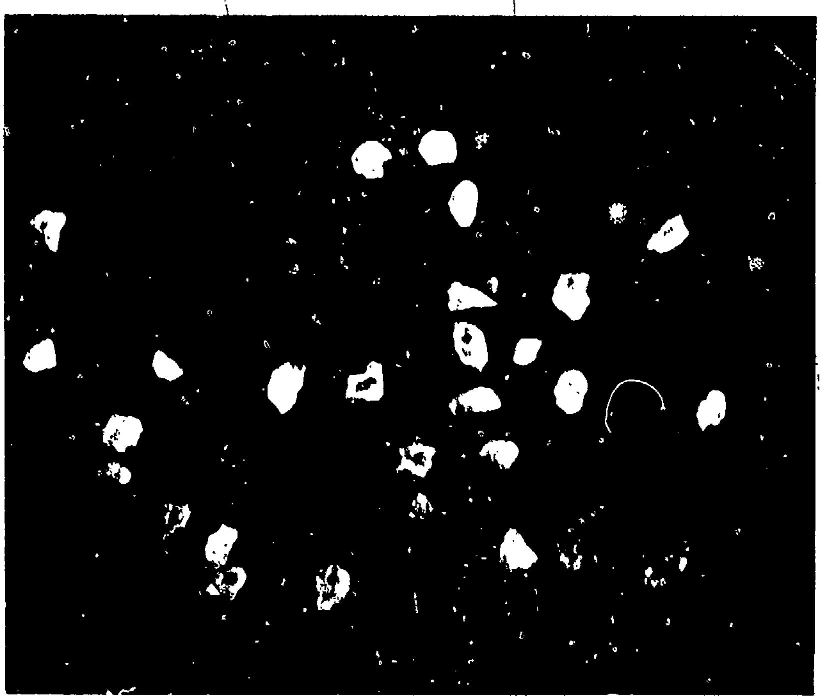

5482-2B 40X

Figure 2. Quartz Particles Separated from Powder Lot 106.

Table I

EMISSION SPECTROGRAPH IMPURITY ANALYSIS OF ALUMINA POWDER*

Impurity Element	Concentration Lot 106 ppmw	 Lot 119 ppmw	 Lot 120 ppmw
Mg	<1	1-10	1-10
Ca	ND	1-10	1-10
Si	1-10	10-100	10-100
Fe	1-10	1-10	1-10
Cu	<1	<1	<1
Ga	1-10	1-10	1-10
Pb	1-10	ND	ND

*Vendor I

become clearer in the next section where defects with a SiO_2 origin are found in a billet fabricated from Vendor II powder.

It is recognized that contamination during consolidation processing can also contribute to the defects discussed in fabricated billets. However, every possible precaution was employed to insure the validity of the powder analyses as representing the "as-received" analysis.

C. General Defect Analysis

A number of hot pressed Al_2O_3 billets were examined for Type I defects by a variety of microscopy and analytical techniques. An attempt has been made to categorize the predominant defects.

1. Spherical Shade Zones

Defects in this category contained no obvious inclusions as detailed by optical microscopy and were one of several shadings relative to the matrix; light color spheres with no distinct boundary, dark color spheres with no distinct boundary, and light color spheres with a distinct ring and halo effect. The latter defects are illustrated in Figure 3. X-ray analysis was performed on one of the isolated defects illustrated and compared with analysis of the matrix. No phase composition differences were detected as α-Al_2O_3 was the major phase, and $MgAl_2O_4$ was a minor phase. Several weak unidentified lines similar to the patterns identified as $Na_4O_2O_7 \cdot H_2O$ from powder lot 106 were observed in both analyses.

Scanning electron microscopy and microprobe studies were performed at Naval Armor Depot* on six spherical defects. The defects ammunition appear to be characterized by increased porosity and often a central large pore cavity as illustrated in Figure 4. The microprobe scans of the defect area detected increased Si and C over the matrix on four defects, increased Si only on one defect, and no impurity on the last spherical defect. The coincidence of Si and C is interesting as C will reduce SiO_2 at 1525°C (near the temperature of hot pressing). Although fabrication is conducted in graphite dies, C is not in contact with interior regions of the billet. A CO/CO_2 mixture is the predominant gas in ambient graphite die hot pressing[2]. It is probable that the CO/CO_2 ratio is at the equilibrium value for the reaction:

$$2\,CO = C + CO_2 \qquad \Delta F^o = 34{,}400 \text{ cal/mole} \qquad (1)$$

At 1800°K the equilibrium constant K_1 is $10^{-4.17}$, and for the condition $P_{CO} + P_{CO_2} = 1$ atm., this gives $P_{CO} \simeq 1$ atm. and $P_{CO_2} = 10^{-4.17}$ atm.

The potential reaction of interest is

$$SiO_2 + 4CO \longrightarrow SiC + 3CO_2 \qquad \Delta F^o_{1800^oK} = +96{,}400 \qquad (2)$$

where $K_2 = 10^{-11.7}$. Assuming an activity of unity for SiC and SiO_2 at

---

*Examination performed under the guidance of M.I.T. Instrumentation Lab by T. Ellis, NAD, Crane, Indiana.

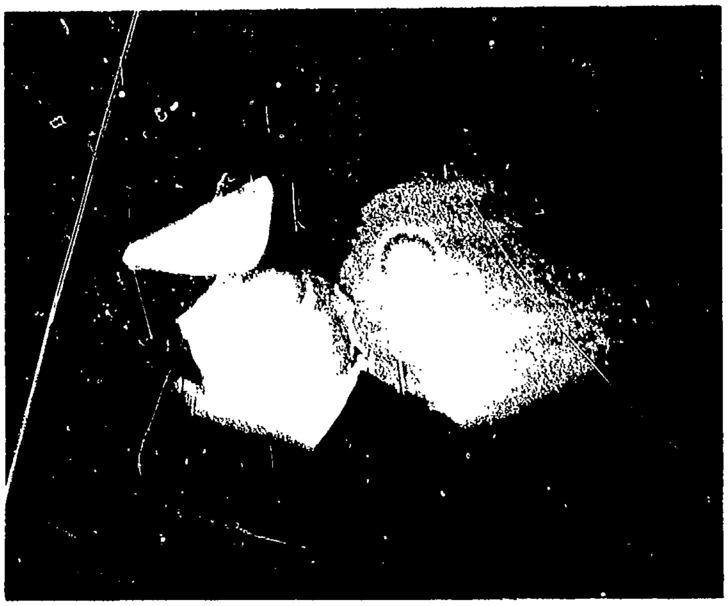

5482-5 40X

Figure 3. Spherical Shade Zone Defect in Billet Pressed from Lot 85 Powder.

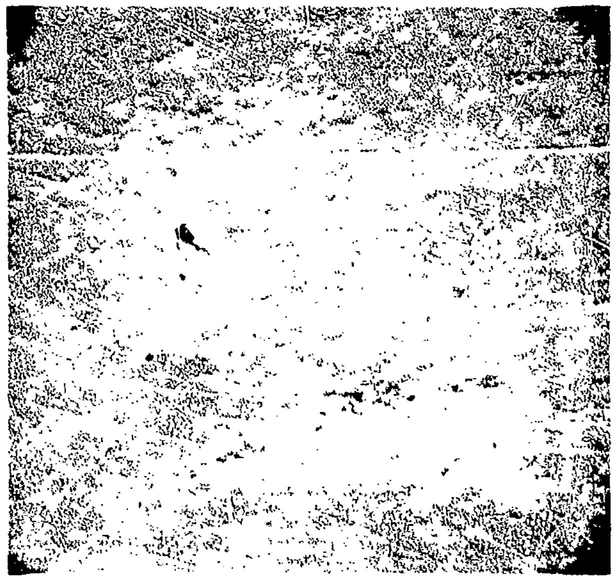

#5-Area 2 (a) 600X

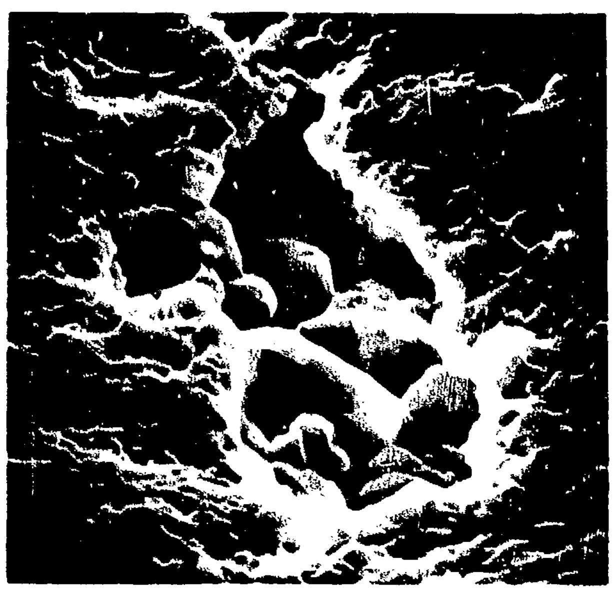

#5-Area 2 (b) 3000X

Figure 4. Scanning Electron Micrographs of Spherical Defects Showing Porosity and Pore Cavity.

equilibrium

$$\frac{(P_{CO_2})^3}{(P_{CO})^4} = 10^{-11.7} \qquad (3)$$

However, due to reaction (1)

$$Q = \frac{(P_{CO_2})^3}{(P_{CO})^4} = \frac{(10^{-4.17})^3}{(1)^4} = 10^{-12.61} \qquad (4)$$

thus,

$$Q = 10^{-12.61} < 10^{-11.7} < K_2$$

meaning that reaction (2) will proceed to the right. At high pressures, which certainly are present within the pore structure, reaction 2 would be further enhanced, thus the presence of C within these defects can be explained as due to a reaction of SiO_2 with CO to form SiC. If N was present, the tendency for the reaction to proceed would be lessened, but it is still expected to be favorable.

2. Second Phase Inclusion

Several examples of second phase inclusions were found. An example of one such inclusion that was isolated by sectioning is shown in Figure 5. A spherical shading zone is associated with this type of defect, but the central large grain was the point of interest. The grain shown in Figure 5 was chipped out and identified as α-quartz by x-ray diffraction. This result correlates with the powder analysis except that the particular billet from which this was extracted was fabricated from Vendor II powder.

Figure 6 illustrates a second inclusion morphology in hot pressed Al_2O_3. This linear defect is probably related to either the metallic or organic fibers shown in Figure 1.

Earlier studies have shown that graphite can become included in hot pressed Al_2O_3. Great care must be exercised in die loading to prevent this contamination and, based on this study where no clear examples of graphite inclusions were found, this source of defects can be prevented.

3. Exaggerated Grain Growth

Alpha Al_2O_3 grains, which are much larger than the matrix, are considered potential flaws as once they became carcked they would demark the critical crack length as defined by the Griffith criteria. Figure 7 illustrates a zone of α-Al_2O_3 grains 170 microns long in a billet made with lot 120 powder. No spinel was detected in these grains although an independent x-ray analysis of the matrix showed two lines identifiable as $MgAl_2O_4$.

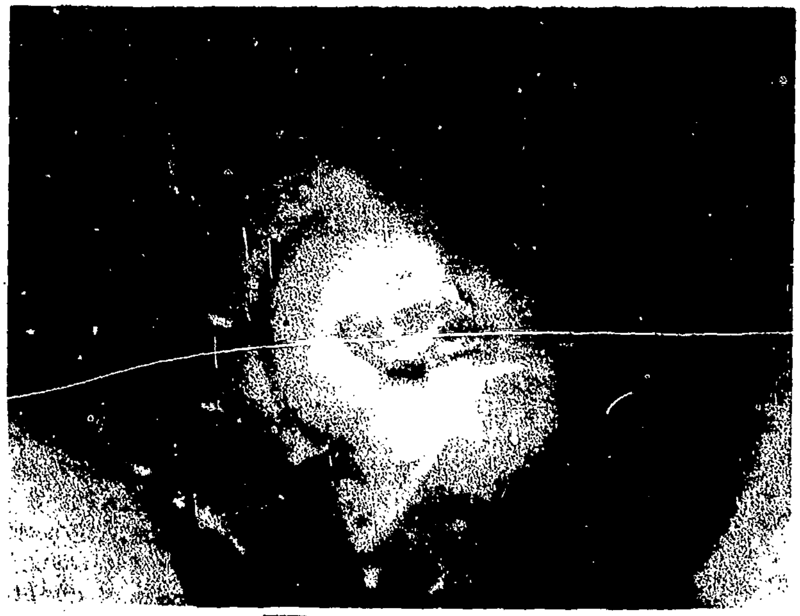

5482-9B

200X

Figure 5. Second Phase Inclusion Identified as α-Quartz from Billet Fabricated from Linde A (polarized light).

5517-3

100X

Figure 6. Linear Defect in Hot Pressed Al_2O_3 Not Positively Identified but Probably Related to Fibers Found in Powder.

4. Fine Grain Region

Figure 8 illustrates a zone of fine grains which appear to be poorly bonded and porous. The size of this defect is only several matrix grain diameters, thus it is much smaller than the spherical shade zones previously discussed. This fine grain defect is thought to be a pocket where agglomerate bridging has prevented adequate particle contact for solid state diffusion, sintering, and grain growth. There is no evidence that this defect has a chemical origin.

D. Hot Pressed Alumina for Testing

Billets for the mechanical test program were fabricated from Al_2O_3 reported to be 99.98% pure by the powder supplier. Several variables were introduced into the test matrix by the billet selection. This is best explained in conjunction with Table II. Grain size is reported as 1.5 the linear grain intercept. Introduction of the FLU billet permits a comparison of material made with Vendor II versus Vendor I powder. However, coupled with this comparison is the fact that none of the Vendor I powder billets employed a vacuum pressing atmosphere throughout the process cycle. The comparison of results for 642 and 645 has the fewest potentially mitigating variables, as only the powder lot number is thought to be a significant variable. A comparison of results for 642 and 1570 compares additive species, concentration, and pressing atmosphere, keeping a constant Al_2O_3 powder lot number.

Table II

HOT PRESSED ALUMINA FOR MECHANICAL TEST PROGRAM

Billet Number	Density gm/cc	Grain Size microns	Powder	Additive wt. %	Pressing Atmosphere
FLU	3.979	1.8	Vendor II	0.25 MgO	Vacuum
642	3.969	2.8	Vendor I - 106	0.25 MgO	Argon-Vacuum
645	3.959	1.7	Vendor I - 120	0.25 MgO	Argon-Vacuum
1570	3.970	1.3	Vendor I - 106	0.20 MgO 0.10 NiO	Ambient

E. Transverse Bend Strength and Flaw Analysis

Strength measurements were conducted in four point bending in ambient air with a relative humidity of 55%. The strain rate employed in testing was 6.9×10^{-5} sec^{-1}.

FLU specimens were tested using a rigid alumina knife edge fixture especially designed for high temperature testing. A nickel alloy ball

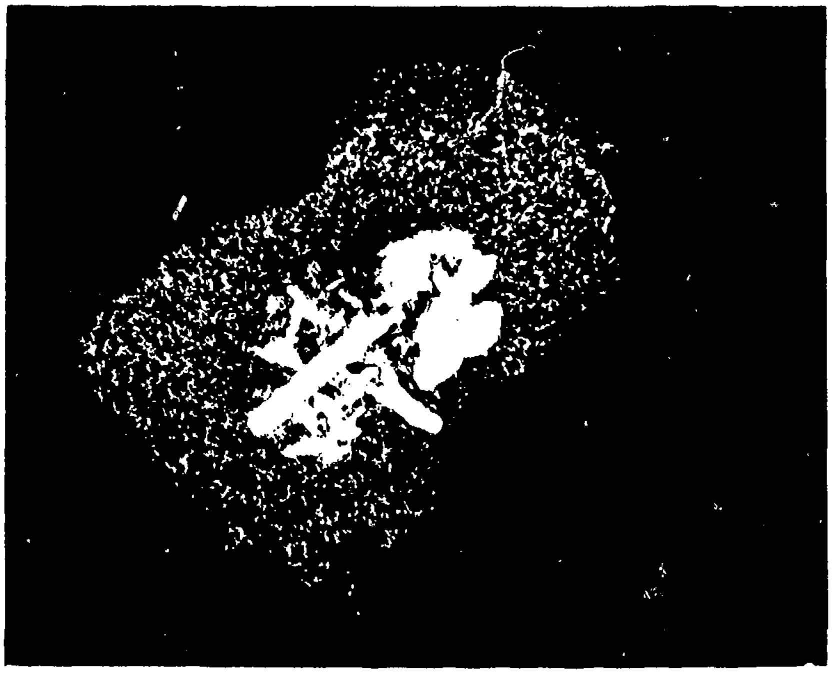

5482-14 144X

Figure 7. Exaggerated Grain Growth of α-Al_2O_3 in Billet Fabricated from Vendor I Lot 120 Powder.

72247 7500X

Figure 8. Fine Grained Porous Weakly Bonded Defect in Billet Fabricated from Vendor I Lot 106 Powder.

bearing and stainless steel fixture was designed and built for the remaining testing, principally to reduce stress concentration and knife edge frictional effects. Consideration was also given to the shifting of the point of tangency at the load and support points. Vrooman and Ritter[3] have shown this to be a serious problem at high deflections, requiring a numerical analysis to obtain corrected stresses. The error in stress for the new roller fixture testing Al_2O_3 at 100,000 psi was calculated to be 0.025%. At this level and with the standard deviations usually found in Al_2O_3 testing, it was considered unnecessary to employ the numerical analysis. Shand[4] has discussed the interpretation of fracture features on glass to include mirror region of smooth crack extension from a flaw, crack branching, and interaction of the crack fr[illegible] with stress waves reflected from nearby surfaces to form Wallner lines. Kirchner et al[5] recently demonstrated that these regions may be identified in polycrystalline Al_2O_3 and are useful in some cases to find the fracture origin. Further, fracture origins could be located in several of their bars. Similer techniques were employed in this study.

Bend strengths are reported in Table III along with the results of a detailed flaw analysis employing a combination of stereo and reflected light microscopy techniques as well as electron microscopy replica techniques. These results are summarized in Table IV.

Figure 9a illustrates the entire fracture face of a specimen in the FLU series. The interpretation of the crack pattern on this fracture surface was that the critical flaw was in the center of the bar's width 4 mm (on the photograph) below the surface. A higher magnification of this region is shown in Figure 9b. By careful fracturing and separation techniques, the flaw was isolated in a small fragment of the matrix material. The x-ray diffraction pattern of this fragment consisted of a fine polycrystalline α-Al_2O_3 pattern with a superimposed "single crystal" α-Al_2O_3 pattern. The fragment was also examined in plain and polarized transmitted light. This showed a very fine grained transparent matrix surrounding 2 or possibly 3 large pale green transparent grains. Throughout each of these grains, very fine opaque inclusions were observed. It could not be determined whether these fine inclusions were crystalline or pores, but the latter appears more likely. Thus, what appeared to be a 75 μ grain was actually 2 or 3 α-Al_2O_3 grains high in impurities.

Figure 10 illustrates a sub-surface fracture origin in a bend bar from the 645 series. This sample was not subjected to the detailed x-ray analysis of the previous sample, but it was thought that a very similar sub-surface secondary grain or perhaps two grains based on electron microscopy was the cause of failure. This single or compound grain was not colored.

An alternate interpretation of flaws of the type illustrated in Figure 10 where corroborative evidence is lacking is that such "grains" might actually be regions of transgranular fracture. Figure 11a illustrates an interesting region at the edge of specimen 642-5, which, at first glance, had the appearance of one large grain. However, the photomicrograph and electron microscopy examination (11b) show many grains within this region with a grain size a factor of four larger than the matrix. This was the

TABLE III

FRACTURE STRENGTH AND FLAW ANALYSIS

Specimen Number	Bend Strength Kpsi	Observations
FLU-1a	46	Black colored inclusion at fracture origin.
FLU-3a	77	Fracture origin at a large grain.
FLU-4a	77	Black inclusion at fracture origin.
FLU-6a	48	Large grain at fracture origin.
FLU-7a	78	No obvious flaws at fracture origin; however, several very small black spots in the general area.
Average -	65.24	
Standard Deviation -	14.9	
642-1	89.0	Fracture origin either large grain or oblong 15 μ patch of fine grains.
642-2	95.0	Double fracture; one fracture origin large grain, other origin oblong 15 μ patch of fine grains.
642-3	89.0	Fracture origin one of following; longitudinal surface scratch, red inclusion, black inclusion.
642-4	95.3	Fractured outside gage length. Fracture origin possible large grain.
642-5	91.4	Fracture origin at large grain.
642-6	86.0	Fracture origin at oblong 15 μ patch of fine grains.
Average -	91.0	
Standard Deviation -	3.4	
645-1	48.6	45° surface scratch interacting with fracture origin.
645-2	41.4	Either black inclusion or large grain as fracture origin.

TABLE III cont.

Specimen Number	Bend Strength Kpsi	Observations
645-3	53.3	Broke outside gage length. 45° surface scratches interacting with fracture origin.
645-5	77.3	Black inclusion at fracture origin.
645-6	70.1	No flaws located.
645-7	63.1	Sub-surface spherical shade zone as fracture origin.
645-8	65.7	Black inclusion at fracture origin.
645-9	65.7	No flaw located, corner fracture origin.
Average -	60.65	
Standard Deviation -	11.2	
1570-1	82.7	Fracture origin at corner. No flaw located.
1570-2	57.8	Fracture origin at corner. No flaw located.
1570-3	71.7	Fracture origin at corner. No flaw located.
1570-4	88.7	Fracture origin at center. No flaw located.
1570-5	49.8	Possible large grain at fracture origin. Also 60° surface scratch interacting with fracture origin.
1570-6	40.8	40° surface scratch interacting with fracture origin.
Average -	65.34	
Standard Deviation -	7.3	

Table IV

SUMMARY OF FLAW ANALYSIS

Billet	No. of Tests	No Flaw Located	Large Grains	Black Inclusion	Oblong Fine Grain Region	Spherical Shade Zone	Surface Scratches
FLU	5	1	2	2	0		0
Average Strength, Kpsi	65.2	78.0	62.5	61.5			
642	6	0	2	1	3		0
Average Strength, Kpsi	91.0		93.8	89.0	90.0		
645	8	2	1	2	0	1	2
Average Strength, Kpsi	60.7	67.9	41.4	71.5		63.1	50.9
1570	6	4	1	0	0		1
Average Strength, Kpsi	65.3	75.2	49.8				40.8
Frequency of Occurrence in Total Testing		28%	24%	20%	12%	4%	12%

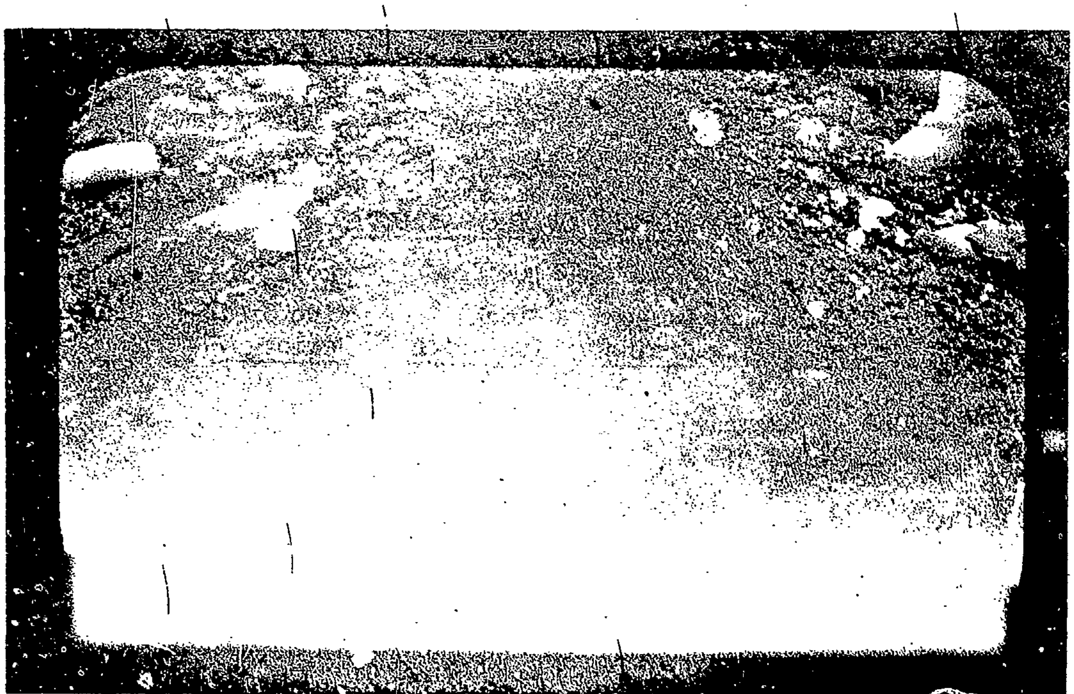

5517-4 (a) 20X

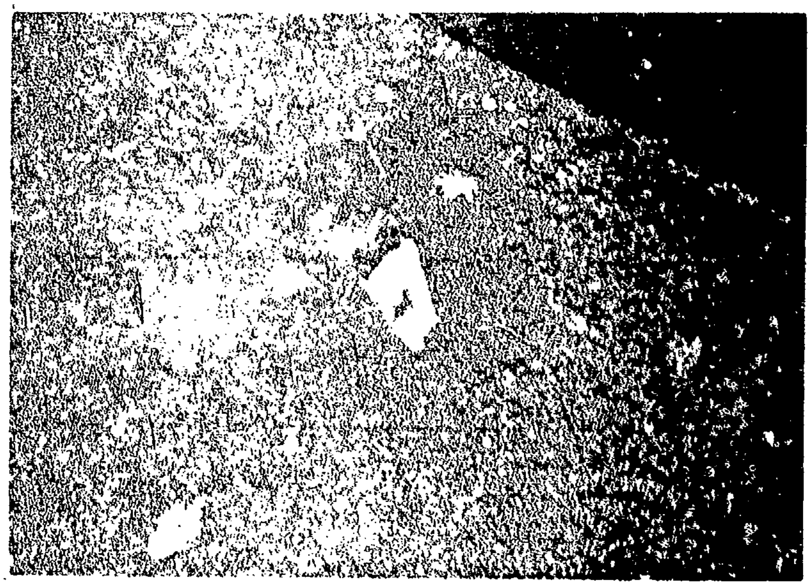

5517-5 (b) 150X

Figure 9. Bend Specimen [illegible] Showing (a) Entire Fracture Surface, and (b) Dark Colored Grain at Fracture Origin.

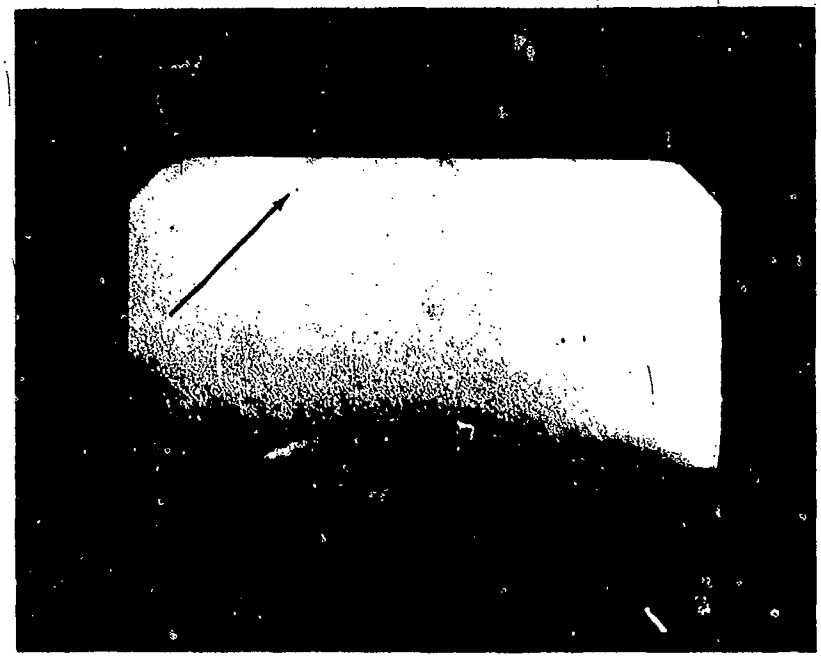

5594-7 (a) 15X

5594-7 (b) 500X

72260 (c) 7500X

Figure 10. Specimen 645-2 Showing (a) entire fracture face with flaw arrowed, (b) higher magnification optical views, and (c) electron micrograph of secondary grains presumed to be the critical flaw.

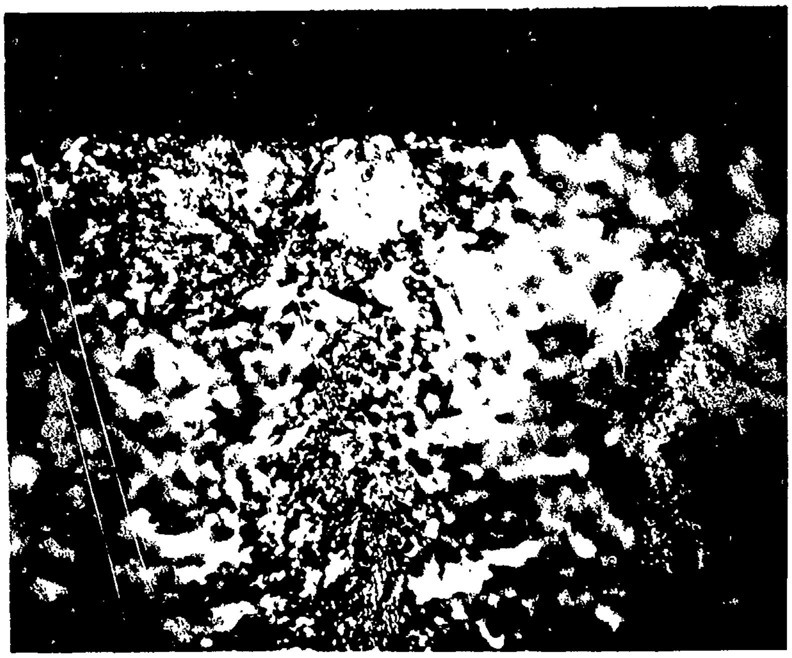

5594-5 (a) 500X

72250 (b) 7500X

Figure 11. Mirror Zone at Edge of Specimen 642-5 (a) exhibiting similar appearance to large grains, and (b) electron fractograph of zone indicating a moderately fine grain size and transgranular fracturing.

closest example found to the classic mirror fracture in glass.

The inclusions found as fracture origins were categorized as "dark" inclusions and although most were black, a few red particles were seen. None of the inclusions observed at fracture origins were linked conclusively to the SiO_2 inclusions discussed in Section C2. Detailed structural and chemical analyses were not carried out on most of these flaws. In one case where a detailed analysis was conducted, what at first appeared to be a single dark inclusion, was found to consist of several colored α-Al_2O_3 grains (see discussion pertaining to Figure 9). Another fracture origin flaw thought to be an inclusion is shown in Figure 12.

Only one white spherical shade zone was found as a fracture origin in this test series. This was not photographed. However, a flaw fracture origin similar in appearance was photographed from another FLU test series, and is shown in Figure 13.

Billet 642 had a high incidence of oblong fine grained defects at the fracture origin. Figure 14a illustrates a macroscopic view of specimen 642-2. At higher magnifications, the fracture surface was indistinct, so the tensile surface was polished to intersect the flaw. Several specimens with similar flaws were polished before obtaining a suitable polish. Figure 14b illustrates the appearance of the flaw, and one is illustrated similar in appearance to that shown in Figure 14a. The area having the appearance of $\frac{1}{2}$ of an oval is the flaw origin. The edge was difficult to prepare, thus it is uncertain whether or not the area was porous; there is a strong possibility that this is the case. Figure 15a is a polarized light photomicrograph of the same flaw shown in Figure 14b clearly outlining the extent of what can be identified as a second phase. Further evidence for a second phase is shown in Figure 15b where this area was lightly etched with phosphoric acid. The second phase zone has been selectively attacked leaving a few lightly etched grains of the second phase and a matrix that is virtually unetched. Thus the defect appears to have a chemical origin and is not related to the fine grain unbonded regions shown in Figure 8.

Several specimens had fractures that were identified as originating from surface scratches. Figure 16 illustrates the basis for such a conclusion on a specimen 1570-6. The flaw origin identified on the basis of the crack pattern in Figure 16a matches the scratch 45° to the bar axis shown in Figure 16b. These scratches were inadvertently introduced on several bars during hand honing of the edge radius. This was unfortunate, as the strength-flaw analysis showed them to be the most serious flaw encountered.

F. Discussion

The Vendor I powder analysis revealed an extremely critical problem. Any of the non-alumina contaminants are thought to be potential sources of flaws. Even an organic fiber could burn out during processing leaving behind a zone of poor bonding as Figure 6 suggests. In addition, a fiber could leave behind a C residue which might react with SiO_2, for example. The presence of large α-quartz grains was clearly the most disturbing

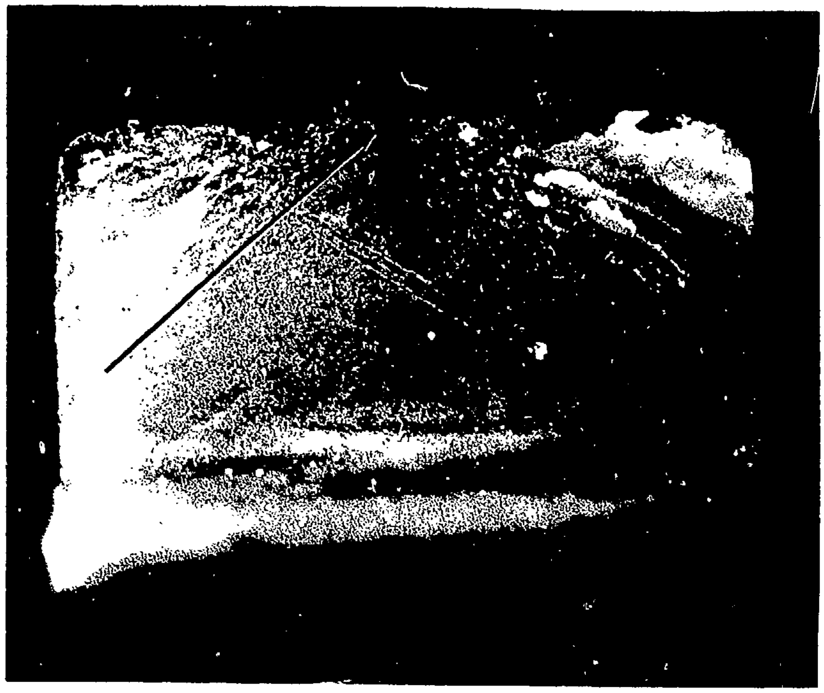

5594-15 15X

Figure 12. Flaw Origin Occurring at a D[illegible] Inclusion in FLU 2-la.

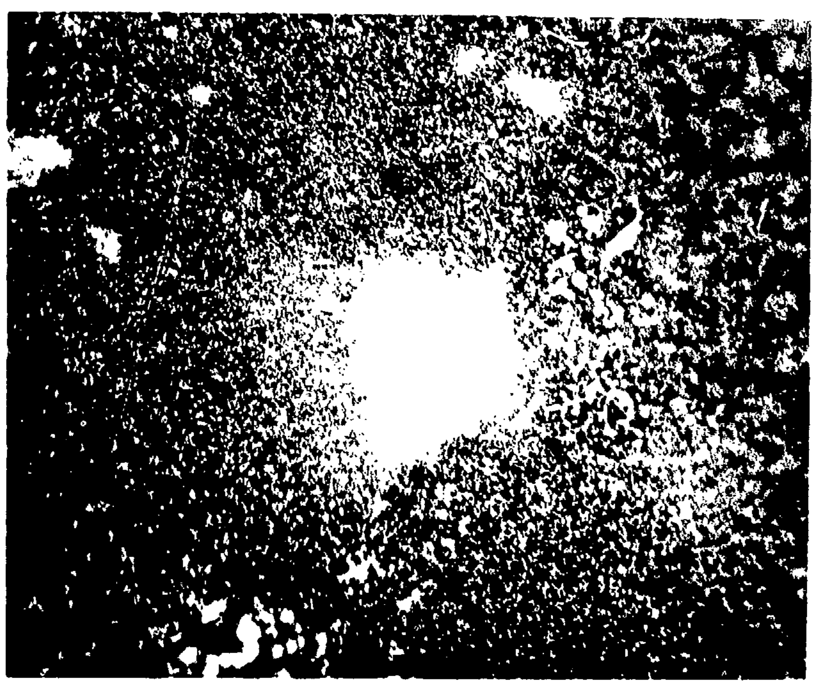

5594-12 250X

Figure 13. Flaw Origin Occurring at White Spherical Shade Zone in FLU-3-1V.

5594-3 (a) 15X

5594-2 (b) 250X

Figure 14. a) Fracture face in billet 642-2 of specimen having oblong flaw, and b) polished face normal to fracture face.

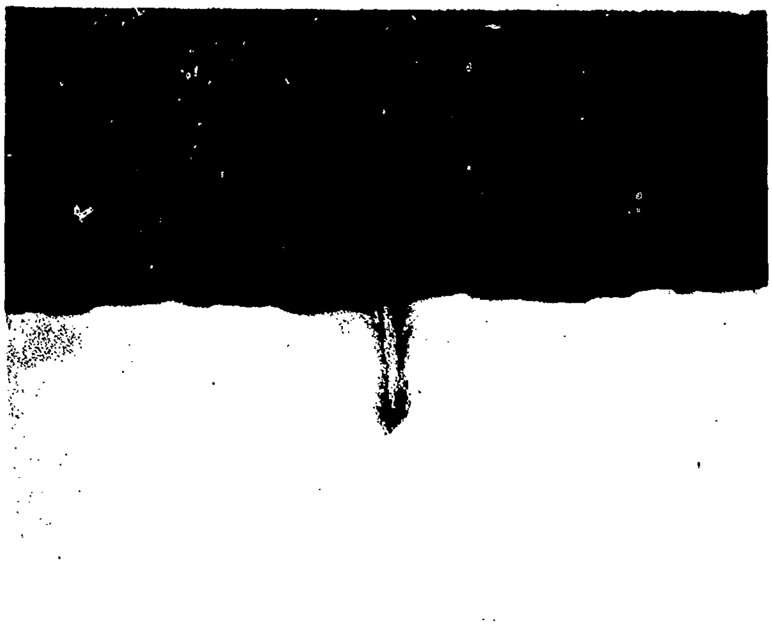

5594-1 (a) 250X

5594-6 (b) 250X

Figure 15. Section normal to fracture face on 642-oblong patch flaw viewed a) polarized light, and b) after light etch.

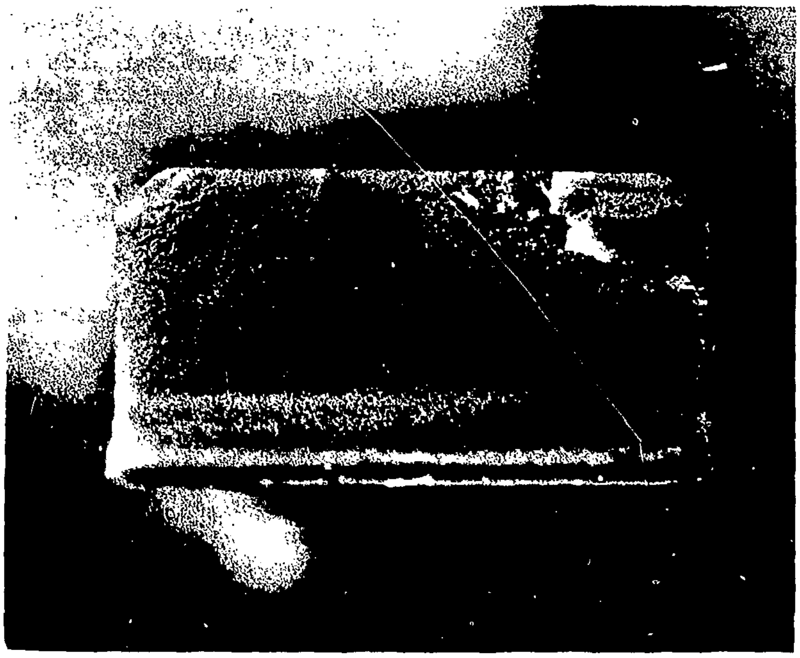

5594-8 (a) 15X

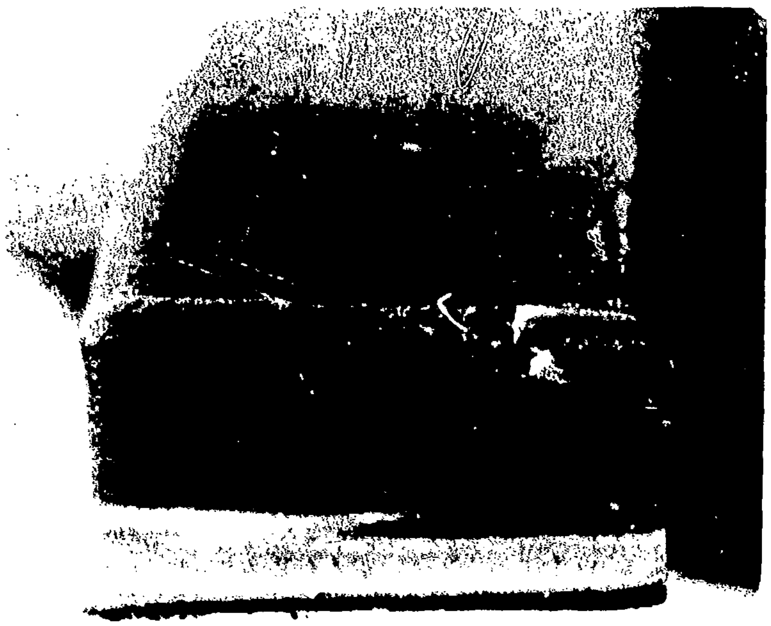

5594-9 (b) 15X

Figure 16. Specimen 1570-6 showing a) fracture origin, and b) correlation of 45° surface scratch with fracture origin.

finding, as SiO_2 was linked to defects in hot pressed billets. This level of contamination is truly remarkable in a powder giving 1-10 ppm impurity analysis for this element, and leads to the view that emission spectroscopy is an extremely selective analytical technique. Subsequent analysis of a SiO_2 inclusion in a billet made from Vendor II powder leads to the conclusion that such impurities can be present in powder from both vendors. The production of high quality Al_2O_3 bodies will require either finding a source of inclusion-free Al_2O_3 powder or encouraging the present manufacturers to exercise scrupulous care in powder production.

Inclusions can be introduced during consolidation processing. Examples of this have not been clearly defined during this study, but previous work in hot pressing Al_2O_3 has shown the necessity of establishing procedures for eliminating particulate carbon as an in-process inclusion.

Spherical shade zones probably are of several different origins. They appear to be slightly higher in porosity than the matrix, and it is thought that many have a chemical origin. Apparently an impurity singularity undergoes a chemical reaction and affects a spherical zone surrounding it. The center of the sphere is quite porous. Only one example of this defect as a fracture origin was encountered in the mechanical testing. These defects were widely spaced reducing the probability of them being in the zone of maximum stress. This does not mean that such defects can be ignored or minimized as applications such as gas bearings and substrates require highly perfect defect-free surfaces.

Second phase inclusions, particularly in the case of SiO_2 are, in some cases, similar to the spherical shade zone defect. The second phase is either of a large particle size so the reaction is incomplete during the thermal cycle or the phase is thermodynamically stable. An example of the former case is the large α-quartz grain in Figure 5, and an example of the latter condition is $MgAl_2O_4$ which showed upon x-ray analysis several times. It should be noted that $MgAl_2O_4$ was never specifically identified with an observable defect. Ball milling the powder is thought to be beneficial. This reduces the particle size of inclusion contaminants and uniformly distributes the grain growth inhibitor. It is thought that a finely divided SiO_2 will react to form $2SiO_2 \cdot 3Al_2O_3$ as a thin grain boundary second phase which would be preferred over a large α-quartz inclusion. The grain boundary phase would still represent a source of weakness as the grain to grain bond strength would be reduced over a pure Al_2O_3 system. $MgAl_2O_4$ second phase is observed more frequently due to MgO being added in a concentration exceeding its solid solubility level than as a result of nonuniform mixing of the MgO. Based on the work of Roy and Coble[6], it is estimated that the solid solubility for MgO is 0.0086 wt. % at 1500°C. The results of this work probably underestimate the amount of that which can be distributed in 2 um grain size Al_2O_3 at 1500°C. There is some uncertainty of the grain size for the Al_2O_3 used in the 1530°C solubility measurements by Roy and Coble. A calculation of the number of Mg^{+2} ions at the grain boundary of 2 um grains, assuming a monolayer saturation, places the solubility for this at 0.0338 wt. %. It is unclear if the 0.0086 wt. % measured by Roy and Coble should be added to the 0.0338 wt. %. It is clear in any event that the 0.25 - 0.3 wt. % of grain growth inhibitor used should and does produce a second phase. This level of additive historically evolved from

sintering studies conducted at much higher temperatures where solid solubility was greater. The presence of $MgAl_2O_4$ cannot be beneficial for mechanical behavior; thus, it is concluded that lower levels of additive must be tried.

There are several possible explanations for exaggerated grain growth in hot pressed material. Since MgO is added as a grain growth inhibitor, one explanation is that the MgO was not uniformly distributed and that the grains grew by the classic exaggerated grain growth mechanism. The fabricated process included a 16-hour wet ball milling as the manner of mixing the MgO, which is usually considered to be a very efficient and thorough manner of mixing. A second possible explanation is that impurities were clustered in a local volume and promoted grain growth to the point where exaggerated grain growth took over, resulting in the very large grains shown. For the one case illustrated in Figure 9 where a large colored 2-3 grain region was found, impurity promoted grain growth is the most probable mechanism. It is suspected that nonuniform mixing of the grain growth inhibitor may have been involved in some of the other secondary grains observed.

The flaw analysis shown in Table IV demonstrated that surface scratches at an angle to the specimen axis result in the greatest strength reduction. This result is consistent with Rice's[7] work in which he showed that oxide bend specimens ground normal to the specimen axis were markedly weaker than specimens ground with the final passes parallel to the specimen axis. This is apparently due to the increased crack width relative to the stress field and a commensurate increase in stress concentration. In the case of the scratches observed in test specimens from this program, the scratches also appeared deeper than the parallel grinding damage which further accenuated the flaw. It was quite noteworthy that this type of surface damage produced a greater strength reduction than any of the other flaws discovered. Only one specimen containing a deep angled scratch was observed which had a fracture origin other than the scratch.

The next most serious flaw was large secondary grains. It was interesting to note that these flaws could act as volume flaws as in several cases they were many grains below the surface. Thus the strength could be expected to be dependent on the volume under test as predicted by Weibull and experimentally verified by Pears and Starrett[1]. This could explain the bimodal strength-frequency plot noted on one set of specimens by these researchers. Some researchers have predicted that Al_2O_3 would have strength statistics governed by surface area Weibull statistics. Volume statistics would be expected to apply based on results of this program. For several flaws encountered in this program, the grain size and position below the surface were measured. The calculated stresses at the flaws are plotted in Figure 17, where all data has been corrected to grain size (1.5 grain intercept). The fracture stress values are intermediate between the grain size - strength curve for hot pressed Al_2O_3 where billets were annealed for grain growth then machined by Passmore, Spriggs, and Vasilos[8], and the curve for as-sintered surfaces on Al_2O_3 by Charles and Shaw[9]. They coincide quite closely with the data of machined hot pressed Al_2O_3 followed by annealing for grain growth by Spriggs, Mitchell, and Vasilos[10]. The coincidence appears reasonable as an internal large grain could be expected to have a flaw size closer to a sample where diffusion may have healed grinding damage cracks compared with an as-machined sample of the same grain size where grinding

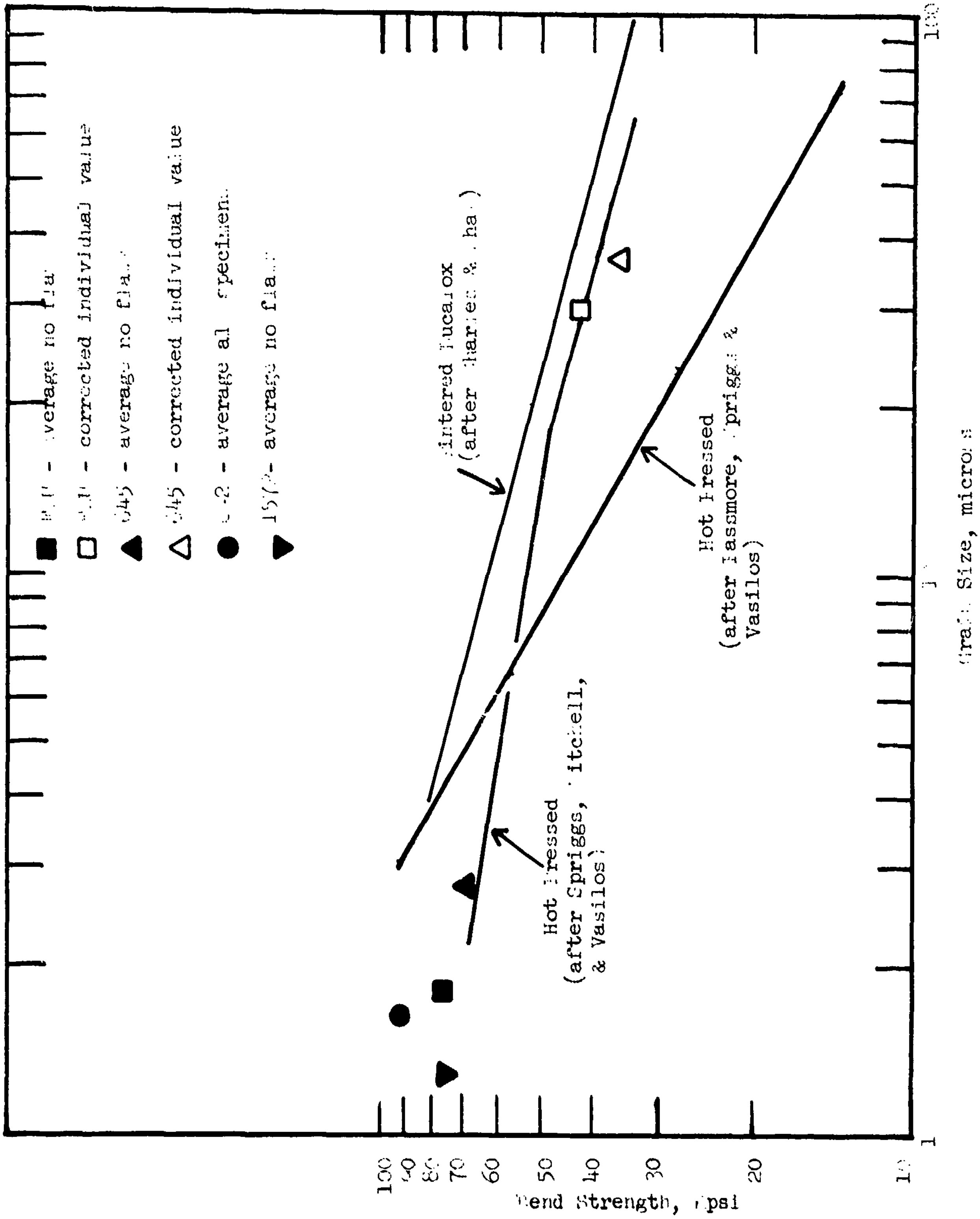

Figure 17. Room temperature bend strength for flawed and unflawed specimens compared with literature data.

damage is expected to have cracked surface grains to at least one grain depth. The question of how a crack was initiated in an interior large grain is interesting and probably very complex. One possibility is the anisotropic thermal expansion of large grains compared with the matrix.

The flaw designated as an "oblong fine grain region" was shown to have a chemical origin as it clearly contains a second phase. Thus, in terms of the flaw analysis, this flaw should be added to the "black inclusions" resulting in a 32% frequency of occurrence for chemically derived inclusions as the strength limiting flaw. It is interesting to note, however, that in billet 645 the strength was actually higher by 3 Kpsi for the specimens with an inclusion than for the apparently unflawed specimens. Specimens in the FLU billet were just reversed in that the unflawed specimen was 17 Kpsi stronger than the one containing a black inclusion at the fracture origin. Two thirds of the specimens in billet 642 contained inclusions, yet this was the strongest billet by a significant margin. Also, the standard deviation is least for this billet. This latter fact was partly due to the observation that the same kind of flaw was controlling most of the fractures. In the general defect analysis it was noted that large particulate SiO_2 was a major contributor to inclusion and spherical shade zone defects. Although SiO_2 was not specifically linked to defects having a chemical origin in the bend bar analysis, it is suspected as having caused some of the defects noted.

A comparison of the strength results for the FLU billet made with Vendor II powder and billets 642 and 645 made with Vendor I powder gave mixed results, leading to the conclusion that one manufacturer's powder is not necessarily preferred over the other. The powder lots tested seem to suffer deficiencies characteristic of the time they were produced. The two Vendor I powder billets,642 and 645, hot pressed by the same process, exhibited quite different strength and flaw differences. This suggests that lot to lot powder variability may be a significant factor in determining properties of the hot pressed product. This, of course, has serious implications in terms of producing an alumina body with a consistent strength or a reproducbile high strength value that can be used for design purposes. The powder lot used (106) to produce the higher strength billet (642) had a lower Si analysis by emission spectroscopy. Even though it has been argued that emission spectroscopy is a highly selective analytical technique, the Si analysis apparently can be taken as an indication of the quality of the powder lot. Based on a comparison of the average strengths of 642 and 1570 where the main variable was the atmosphere during pressing, it was concluded that the vacuum-argon atmosphere gives a strength advantage. This is consistent with the work of Rice[11] relating strength in hot pressed Al_2O_3 to gas phase entrapment. The ambient hot pressing atmosphere would be expected to produce a greater gas phase entrapment. This comparison is partially compromised by the fact that additive species and concentration were also varied between 642 and 1570. A greater concentration of free spinel phase or possibly a monolayer of reduced NiO in 1570 could have given the same results, for example. It is important to point out that other variables such as the powder lot may override the pressing atmosphere effect. Note, for example, that 645 (lot 120, argon-vacuum atmosphere) and 1570 (lot 106, ambient atmosphere) show nearly equal average strengths. It is

tentatively concluded that given the highest quality powder lot, an argon-vacuum pressing atmosphere is preferred. It is interesting to note that 642 and 1570 produced with the same powder lot exhibited quite different flow statistics. Billet 642 showed a high incidence of inclusions and 1570 was free of crack initiating inclusions. This suggests that the inclusions noted in 642 are related to the process rather than the powder. This possibility has already been acknowledged several times in this study.

The results of this study bear on the findings of the detailed Weibull analysis of Pears and Starrett[1]. They found an effect of specimen volume on the strength of alumina of the type predicted by Weibull Theory, but a single set of Weibull constants could not be determined from the data. They conducted a fractography analysis forming a basis for elimination of many data points where they observed macroscopic flaws. It is now thought the billets supplied had flaws that varied in flaw density and type. The volume effect on strength would be different for each flaw density-type combination giving a different set of Weibull constants. One set of Weibull constants will be achieved only when the manufacturing of hot pressed Al_2O_3 becomes sufficiently controlled that such variables as shifting from one powder lot to another no longer affects flaw density and type.

Also shown in Figure 17 are the average strengths for the unflawed samples. In the case of billet 642, there were no unflawed samples, so the average strength for the billet was plotted. The data agree best with that of Spriggs et al[10]. Since as-machined surfaces were tested for the present study, it might be expected that the data would better agree with that of Passmore et al[9] where similar surfaces were tested. It should be pointed out that Passmore et al never measured material with as fine a grain size nor achieved strength any higher than 90 Kpsi. The present results appear to support the view that the strength versus grain size curve shows a break at fine grain sizes. This has been taken by some investigators as evidence fo plastic flow contributing to crack initiation.

In light of observations in this study and the work of others, the question of dislocation nucleated versus Griffith flaw nucleated fracture in polycrystalline Al_2O_3 should be re-examined. The Griffith equation for plain stress long elliptical cross section crack is

$$\sigma_f \quad \left(\frac{2E\gamma}{\pi c}\right)^{1/2} \qquad (5)$$

where σ_f is the fracture stress, E the elastic modulus, γ the fracture surface energy, and C the half length of the elliptical cross section.

The dimension C has been related to the grain size with the argument that damage due to machining extends from the surface some depth related to grain size. Grain boundaries are considered to be effective in arresting cracks. The γ quantity contains terms relating to the thermodynamic surface energy, the work to create clevage steps, the work to create secondary cracks, and the work expended by plastic flow.

Carnigilia[12] and others have argued that the crack is nucleated by a dislocation multiplication process at high effective stresses in the small grain size regime and grows to some length related to grain size prior to fracture. A Petch plot of the form

$$\sigma_f = N(\sigma_y) + KG^{-\frac{1}{2}} \tag{6}$$

where $N(\sigma_y)$ is a constant related to the yield stress, K is a constant, and G is grain size, represents the strength data over a range of grain sizes. At large grain sizes after the Petch plot branches, the Griffith criteria were assumed to be controlling fracture in Al_2O_3, MgO, and BeO.[12]

It has been previously noted that γ is a function of grain size and porosity.[13] In general, γ is low at small grain sizes and rises to some maximum at intermediate grain size, only to fall again at large grain sizes. The porosity effect is less pronounced[13]. As can be seen from an examination of equation (5), this could have the effect of producing a break in a σ versus $G^{-\frac{1}{2}}$ plot. The cause of $\gamma = f(G)$ has not been satisfactorily explained, but it would be surprising if it were phenomenologically related to the arguments supporting a dislocation nucleated fracture of polycrystalline Al_2O_3.

This study has shown that a substantial number of fractures were nucleated by flaws many times larger than the grain size. Thus it is suggested that as G decreases, the ratio C/G increases. This fact alone could cause the σ_f versus $G^{-\frac{1}{2}}$ plot to turn over and break at small grain sizes. Coupled with this effect, it was noted that many fractures originated from sub-surface flaws. The effective crack length would be halved compared to the same flaw at a surface site. Further, the crack geometry may be different from a surface flaw going from an elliptical to penny-shaped crack or vice-versa. The penny-shaped crack requires about 60% greater stress for propagation.

Thus, five possible explanations for a break in the room temperature σ_f versus $G^{-\frac{1}{2}}$ curves of polycrystalline Al_2O_3 appear to have merit. Restated, they are:

(1) $\gamma = f(G)$

(2) $C/G \gg$ as $G \ll s$

(3) effective $C > 2C$ for internal flaws

(4) elliptical to penny-shaped as $< G$

(5) σ_g (slip) exceeded

Direct evidence has been found for (1), (2), and (3). Mechanisms (1) and (2) predict a lower strength as observed, while mechanisms (3) and (4) predict a higher strength if the fine grain is the effective flaw. While the possibility of mechanism (5) cannot be discounted, the evidence supporting the Griffith criteria appears to be strengthened.

G. Conclusions

1. Organic and inorganic contamination found in commercially available 99.98% Al_2O_3 powder from two sources leads to inclusions and/or flaws in hot pressed Al_2O_3. Ball milling is an effective processing step for minimizing the size of contaminant particles and, therefore, the resulting flaw.

2. Spinel was found as a second phase by x-ray techniques, thus establishing that 0.25% MgO is too high a concentration when the maximum thermal excursion is 1500°C.

3. Exaggerated grain growth is a significant defect which is caused by one or more of the following: impurity assisted growth, inadequate mixing of MgO, or the standard exaggerated grain growth phenomenon.

4. Spherical shade zone defects in some cases are a result of an in-process chemical reaction of a contaminant with the matrix. One type appears to be SiC formed from SiO_2 + CO. In other cases, they may be zones of slightly higher porosity.

5. Sixty percent of the fractures could be traced to a defect in the material. The cause of failure could not be found in 28% of the specimens, and 12% of the specimens had flaw origins corresponding to surface scratches oriented 45° to the specimen axis, which were inadvertantly introduced into just these specimens.

6. Forty-five degree surface scratches produced the greatest strength reduction, followed by exaggerated grain growth, second phase inclusions, and spherical shade zones.

7. Crack initiation was correlated with both large grains and inclusions as much as 130 microns below the surface of a bend bar, indicating that Weibull volume statistics would probably apply in a strength analysis of this material.

8. Production of two billets produced from one manufacturer's powder using different lots but identical process conditions resulted in microstructures which were identical on the average, but had quite different strength properties and quite different flawed fracture origins. The powder lowest in Si content gave the highest strength.

9. Hot pressing in a vacuum-argon atmosphere gave a stronger material than an ambient pressed body due to retained gas effects.

10. The highest strength billet was not the billet with fewest observed flaws, suggesting that processing variables such as the atmosphere and dopant concentration affect strength.

11. The break in the Petch plot for polycrystalline Al_2O_3 can be

explained by the dependence of surface energy on grain size, the increasing ratio of flaw size/grain size with decreasing grain size, the longer crack length for internal flaws, a change in stress concentration due to crack geometry, or dislocation nucleated crack generation at high stresses. Experimental evidence for the first three mechanisms lend support to the Griffith fracture mechanism.

III. PRESS FORGING OF ALUMINA HEMISPHERES

A. General

Previous experimental efforts[14] on press forging polycrystalline Al_2O_3 established that high density bodies can be achieved with unique properties. High in-line optical transmissivity is obtained as a result of nearly complete pore removal and high crystallographic texturing. The textured structure is achieved by plastic deformation primarily on the basal slip system. This texture is retained through primary recrystallization.

It was suggested[14b] that the porosity distributed throughout the structure presented preferred nucleation sites for the new generation of grains during recrystallization. This process itself could absorb porosity or the structure could be more susceptible to continued densification due to the nearness of pores to grain boundaries, their potential sink. In-line light transmissions of 60% at 0.7 μ wavelength were achieved for the forged material as compared with a maximum of 20% for the best randomly oriented pore free Al_2O_3 available at an equivalent thickness. This resulted from the preferred basal texture eliminating to a large extent the light diffraction due to birefringence. Inverse pole figures demonstrated that the crystallographic orientation was strong but not perfect. The misorientation undoubtedly accounts for the absence of even higher optical transmission figures.

The second property that was enhanced as a result of forging was mechanical strength. It was found that the strength at -196°C and 1200°C was nearly independent of grain size in the 1-20 micron range[14c,d]. Fracture strengths in the 1200° to 1450°C range were over 50% higher than straight hot pressed material of an equivalent grain size[14a]. However, there was no apparent effect of texture on the plastic properties between 1475-1700°C[14d].

Most recently[14g] the process has been applied to curved shapes, whereas the original effort was confined to flat plates. The thin shell hemispheres forged in the previous program were characterized as having a 120° arc of translucent material, a porous rim with edge tears, and a moderate crystallographic and microstructural texture. The work to be described was centered on improving both the area and degree of optical transmission while continuing process development studies centered around strain rate control, lubrication, and preform specification. The ultimate goal was the achievement of a complex shape by forging having the inherent properties of polycrystalline alumina such as good dielectric behavior, high rain erosion resistance, and the improved optical transparency and mechanical properties of press forged alumina.

B. Raw Materials and Preforms

Vendor I 99.98% Al_2O_3 powder was used for all forging experiments. Section II includes a description of this powder. Two-tenths weight percent MgO was added to an alcohol/alumina slip in a Waring blender. The dried powder was isostatically pressed at 20 Kpsi into cylinders $1\frac{1}{4}$ inches diameter by 3 inches long. These were cut and shaped in the green state into circular right cylinders 1 inch diameter by 1 inch high. Several of the cylinders were shaped to include a 2 inch radius cap. One preform was shaped to fit a 120° arc of the forging die and punch set.

The preforms were fired in H_2 at temperatures from 1100-1600°C which resulted in relative densities from 50% to 96%. It was of interest to forge some of the higher density preforms as they were expected to have closed pores, and H_2 is more soluble in Al_2O_3 than other gases[15]. Thus, any light scattering from entrapped gas molecules could be expected to be reduced.

C. Press Forging Procedure

Forging runs were conducted in an induction heated 75 ton press using standard ambient graphite base hot pressing furnace construction techniques. The forging die was constructed from high strength HPD Poco graphite of a design illustrated previously[14g]. The die was designed to produce a 1.1 inch radius hemispherical cap end with a 0.4 inch high tapered cylindrical skirt. A pinned top ATJ punch was used which allowed hot extraction of the male die. This was thought necessary because of the fracture of an early hemisphere presumably due to cooling contraction on the male punch. The boron nitride die lubricant was sprayed or painted directly onto graphite. In most cases graphite paint was used between the male punch and BN cover coat. Ambient atmosphere forgings were employed which meant that at the forging temperature the atmosphere was predominantly CO with a partial pressure of CO_2 and A. The argon permeated into the cavity from the sight tube where it was employed as a sight tube flush. Also, residual nitrogen was expected.

The die assembly was heated to the forging temperature in about 100 minutes. Upon equilibrating at temperature, the ram travel was initiated and driven by a manual strain rate control. The strain rate during the rapid deflection regime was controlled to between 6×10^{-4} sec^{-1} and 1×10^{-3} sec^{-1}. The above strain rates are the best present estimates of acceptable strain rates in the 1850°C range. Once maximum pressure was reached, the deflection rate slowed down as forging and densification came to a conclusion. The specimen was held at maximum temperature and pressure for some prescribed period of time beyond that where deflection has apparently ceased. Some densification continues by diffusion, and there is some evidence that multiple recrystallizations may take place in this period[14]; thus, a hold of 3-4 hours became standard practice. Upon completion of the run, pressure was released and the male punch extracted.

D. Analysis

The degree of crystallographic orientation is an important

parameter for characterization of the forging process. An orientation characterization technique has been developed[16] which is not as tedious as the construction of a complete x-ray pole figure. It is best termed an inverse pole figure and readily allows an evaluation of relative crystallographic orientation. In this technique, the ratio of x-ray diffraction intensities expressed as

$$R_1 = \frac{f(hkl)}{f_o(hkl)}$$

where

$$f_o = \frac{I(hkl)}{\sum_{hkl} I(hkl)}$$

for a random powder pattern and f is a similar function for a forged sample. Another manner of expressing the orientation effect developed during this present program is expressed as

$$R_2 = \frac{q(hkl)}{q_o(hkl)}$$

where

$$q_o(hkl) = \frac{I(hkl)}{I(006)}$$

for a random powder pattern and q(hkl) is a similar function for a forged specimen. This technique has certain advantages that may prove useful. The intensities are compared with just one peak, the basal (006). Thus, if reflections are masked due to interference, the entire calculation would not be affected as it would when using $\sum_{hkl} I(hkl)$ in the original technique. Also, this method permits the calculation of intensities for just two or three peaks to assess the presence of orientation. And finally, comparisons can easily be made between runs checking for increased or decreased crystallographic orientation.

E. Forging Experiments

The experiments are listed chronologically in Table V. The preform for forging 1576 was a pre-fired 50% dense billet which was machined to conform to the die cavity and male punch over 120° of the hemisphere. The preform was approximately ½ inch thick initially. The forging stuck to the male punch during cool down presumably due to the slightly higher thermal expansion coefficient for Al_2O_3 than for Poco graphite. Although it was cracked, it was quite translucent over 2/3 of the hemisphere. A density measurement on the center section gave a 100% relative density. Physical properties on this forging are reported in Section III F. The die was designed such that a 73% depth of forging was equivalent to a full hemisphere, and a 100% forging was equivalent to 220° of arc or 0.4 inch above a full hemisphere. Thus, the 92% depth of forging achieved for 1576 was considerably above a full hemisphere.

Table V

CONDITIONS AND RESULTS FOR HEMISPHERICAL FORGINGS

Experiment	Powder	Preform Prep.	Preform Density gm/cc	Separating Media*	Temp. °C (correct. 65°)	Pressure Kpsi	Time min.	Density gm/cc	Remarks
1576	M1 0.2 MgO	Cold press Prefire Shape 120° arc	2.0	HTP BN/BN Dylon	1875-1895	6.4	180	3.987 Center 3.670 Edge	Shrunk on male punch, cracked, central 2/3 of arc very translucent, forged to 92% of depth.
1577	M1 0.2 MgO	Cold press Sinter H_2	3.82	HTP BN/BN Dylon	1875-1895	6.4	180	3.946 Entire piece	Crack-free, translucent, central 2/3 of arc forged to 92% of depth.
1593	M1 + 0.2% MgO	Cold press Sinter in H_2	~3.8	BN/BN Dylon	1885	6.4	180	3.886 Entire piece	Stuck in female, one non-catastrophic crack, 90° of hemisphere very translucent, forged to 92% of depth.
1603	M1 + 0.2% MgO	Cold press sinter in H_2	?	BN-Dylon BN-Dylon	1885	6.4	180	3.844 Entire piece	Translucent, edge tears, forged to 75% of depth.
1613	M1 + 0.2% MgO	Cold press sinter in H_2	3.74	BN Dylon/ BN Dylon	1885	6.4	180	3.786 Entire piece	Translucent, circumferential crack, edge tears, forged to 84% of depth.
1666*	M1 + 0.2 MgO	Cold press sinter in H_2	3.77	BN/ BN Dylon	1885	6.4	35	3.801 Entire piece	Circumferential crack, partial forging, forged to 58% of depth
1670	M1 + 0.2 MgO	Cold press sinter in H_2	3.431	BN/ BN Dylon	1885	6.4	225	3.781 Entire piece	Crack-free, except for lip, moderately translucent, forged to 92% of depth.

Table V cont.

Experiment	Powder	Preform Prep.	Preform Density gm/cc	Separating Media*	Temp. °C (correct. 65°)	Pressure Kpsi	Time min.	Density gm/cc	Remarks
1675	M1 0.2 MgO	Cold press Sinter in H_2	3.75	BN/ BN Dylon	1875	6.4	225	3.81 Entire piece	1/3 of arc translucent, edge tears, forged to 75% of depth.
1691	M1 0.25 MgO	None Loose Powder fill	1	BN/ BN Dylon	1565	6.4	150	3.559	Opaque, one section cracked, entire cavity filled.
1722	M1 0.2 MgO	Cold Press Sinter in H_2	3.71	BN/ BN Dylon	1865	6.4	180	3.782	Spherical shade zone, defect on interior, 1/3 of arc translucent, forged to 75% of depth.
1727	M1 0.12 MgO	Cold Press Sinter in H_2	3.90	BN/ BN Dylon	1865	6.4	180	3.874	2/3 of arc translucent circumferential crack, edge tears, forged to 58% of depth.

*Coating for female listed first.

Forging 1577, was a very successful hemispherical forging. The preform for this forging was a 96% dense 54 gram sintered cylinder 1 inch diameter by 7/8 inch high. The temperature was slightly higher than some earlier runs, and it was noted that the BN layer was white, smooth, and unreacted compared with some earlier results where a dark reacted layer was observed. The improved lubrication achieved with this BN-graphite paint system apparently contributed greatly to the success of this run. One other difference for this run compared with 1576 was that the male punch was tapped mechanically after lifting it away from the female punch prior to cooling. This apparently freed the Al_2O_3 piece from the male at the forging temperature and consequently prevented cracking. The forging depth was equivalent to 1576. The skirt was lower density and exhibited edge tears. The forging was sectioned at the full hemisphere level, polished, and is illustrated in Figure 18. The hemisphere was very translucent throughout. The apex was slightly more opaque than the remainder of the surface area. This was thought to be due to a dead zone effect. Most forgings exhibit slightly different structures in a central zone adjacent to the punch centers due to the reduced strain in this region. Several one-eighth inch long cracks extended into the hemisphere from edge tears in the skirt. The deformation-pressure-time plot for this run is shown as Figure 19.

Forging 1593 was an attempt to reproduce the successful forging, 1577. The run conditions were successfully reproduced right up to the point where the male punch was to be extracted 1 inch, tapped and the power turned down. A graphite pin broke preventing the accomplishment of the extraction step. As a result, the hemisphere stuck to the punch. A number of techniques were attempted to free the piece. It was finally removed by heating the piece back up to 1800°C and tapping the die at intervals during the heating step. One non-catastrophic crack was observed which had all the appearances of being a brittle crack (as opposed to a crack occurring during the deformation). Thus, it is thought that the crack developed during the removal attempts. The hemisphere itself was very translucent over about 90% of the surface area. Thus, except for the experimental difficulty noted above, it is thought that the successful forging conditions of 1577 were reproduced with very similar results.

Run 1603 was very similar to the earlier runs except the lubrication scheme was altered slightly. A graphite paint undercoat was used for both male and female die faces. The intention was to increase lubrication over the previous successful runs where the graphite paint had been used just on the male punch. The sample was not forged as fully as 1576, 1577, and 1593, although it just reached the full hemisphere forging depth. Edge tears, which began at a height 7/16 inch from the apex and extended 9/16 inch to the edge, were more severe than experienced on the earlier runs. These were thought to arise early in the forging. The sample was clean and quite translucent for about 150° of the hemisphere. The decreased depth of forging was opposite to the predicted effect and remains unexplained.

Forging 1613 was conducted with a graphite paint undercoat on the male punch only and the usual BN layer on both punches. The strain rate was increased over previous forgings, and the sample forged to 84% of the full forging depth. At a time when the load was between 2 and 3 tons, a non-uniform deflection was noted. This shows clearly in the deflection-pressure-

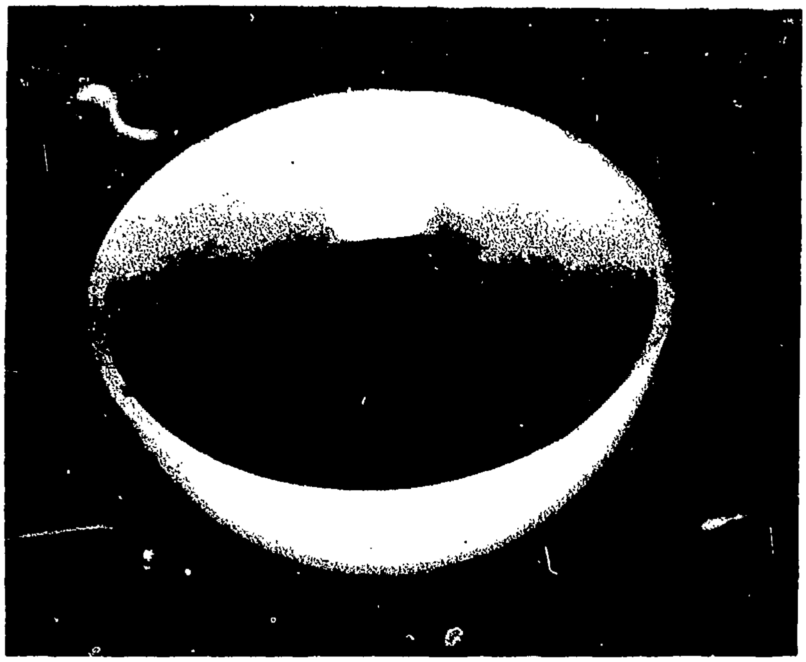

5551-1 $1\frac{1}{2}$X

Figure 18. Hemisphere 1577 Press Forged from Solid Right Cylinder.

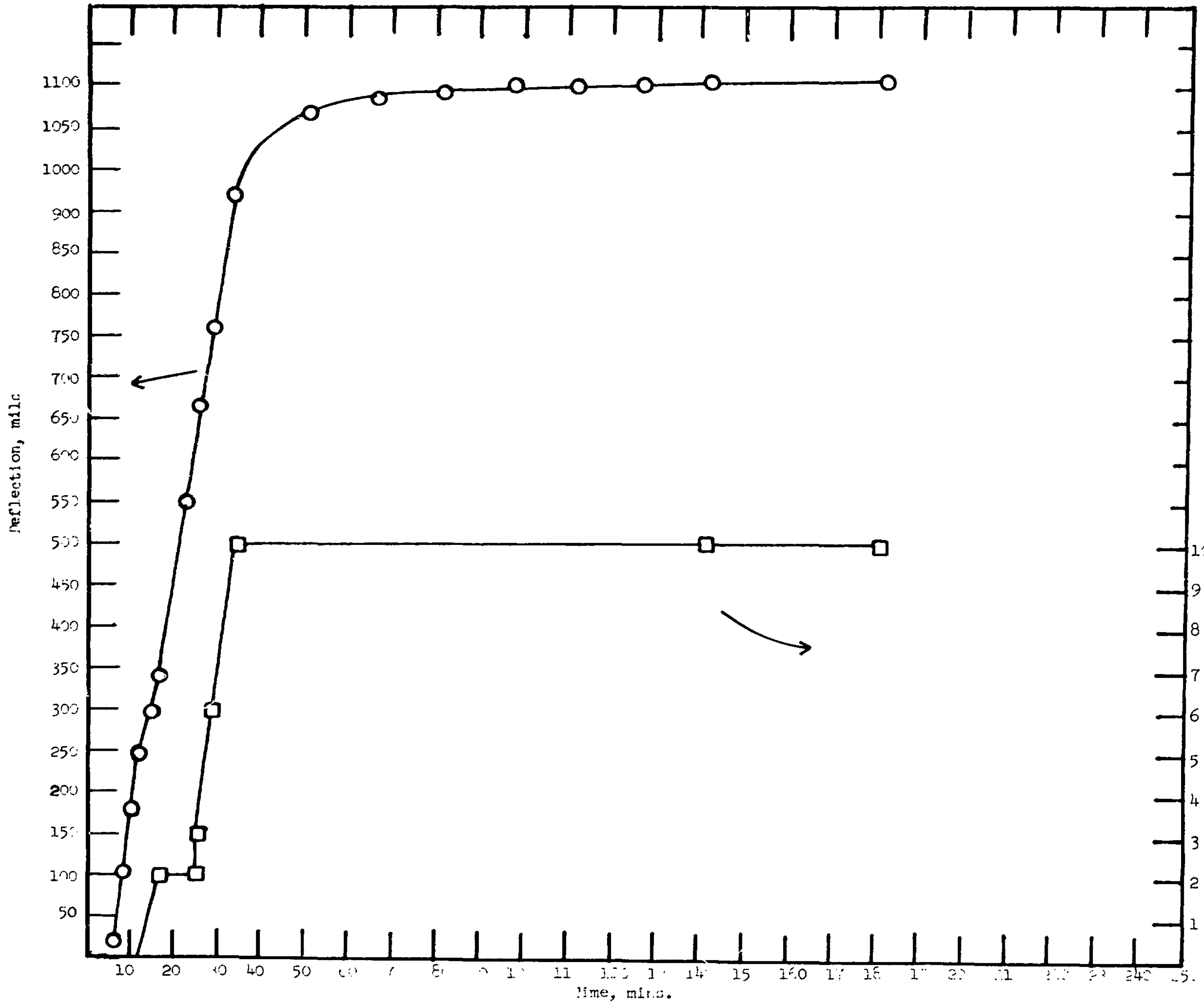

Figure 19. Deformation-Pressure-Time Plot for Forging 1577.

time plot shown as Figure 20. The hemisphere exhibited a circumferential crack $\frac{1}{4}$ inch in height from the apex. Radial cracks extend from this crack to the edge of the specimen. A second run was conducted at this higher strain rate to determine if the cracking was a result of deformation history or perhaps preform strength. At a point about 20 minutes into forging of 1666a, non-uniform deflection similar to that noted for 1613 was encountered. Since it was suspected that cracking had again occurred, the run was terminated after about 35 minutes. This served an additional purpose as plans had already been made to produce a partial forging to study the material flow characteristics. As expected, the piece was only partially forged and exhibited the circumferential crack in an identical position to sample 1613. The deflection-pressure-time plots shown as Figures 19 and 20 were carefully examined and compared. Deflection of between 0.210-0.350 inch occurred due to what is called "pumping action", where the hydraulic system is activated and controlled to give a prescribed deflection rate (0.030 to 0.050 inch/minute). After about 12 minutes of this, it was necessary to apply measurable load to continue forging. In run 1577, the initial deflection rate was 0.050 inch/minute and the load was kept at 2 tons for abcut 10 minutes while the piece deformed at a somewhat reduced rate of 0.020 inch/minute. As the deflection began to slow even further, the load was increased to 3, 5, and 10 tons keeping the deflection rate at about 0.020 inch/minute. On the other hand, run 1613 started off at a rate of about 0.030 inch/minute, was kept at 2 tons only for 2 minutes, and as the pressure was increased above 2 tons, the deflection rate sped up to almost 0.070 inch/minute. Based on similar deformation behavior and cracking for run 1666, it was thought that circumferential cracking occurred immediately after increasing the load above 2 tons due to exceeding the flow stress for the imposed temperature/strain rate/microstructure conditions. These runs effectively established an upper limit to the forging conditions for 94% dense preforms at 1885°C.

Run 1670 was an effort to reproduce hemisphere 1577 and eliminate the circumferential cracking. The deflection rate, as noted in Figure 21, was held at a constant 0.025 inch/minute by incorporating an 8-minute hold at 2 tons. However, after reaching 5 tons cf load, the deflection rate increased to about 0.050 inch/minute for 6 minutes. This forging did not exhibit the circumferential crack and the radial lip cracks were very shallow, indicating that the strain rate control was the critical step in eliminating the circumferential cracks. The sample was quite translucent in the unpolished state, but had a dark surface skirt unlike the best forging. The depth of forging was equivalent to 1576 and 1577.

Forging 1675 was conducted under similar strain rate control conditions during the initial 30 minutes of the run. It was decided to further reduce the strain rate from the 30 minute point on by introducing a hold at 4 tons force and 6 tons force. This had the effect of reducing the depth of forging to 75%. The edge tears were about equivalent to 1576 and 1577. The forging was quite opaque because of the increased wall thickness.

Run 1691 was introduced into the plan as an experiment on the application of normal hot pressing techniques to the production of a hemisphere. Loose powder filled the die and the maximum temperature was 1565°C. The final density was only 89%. Poor pressure transmission in the lateral

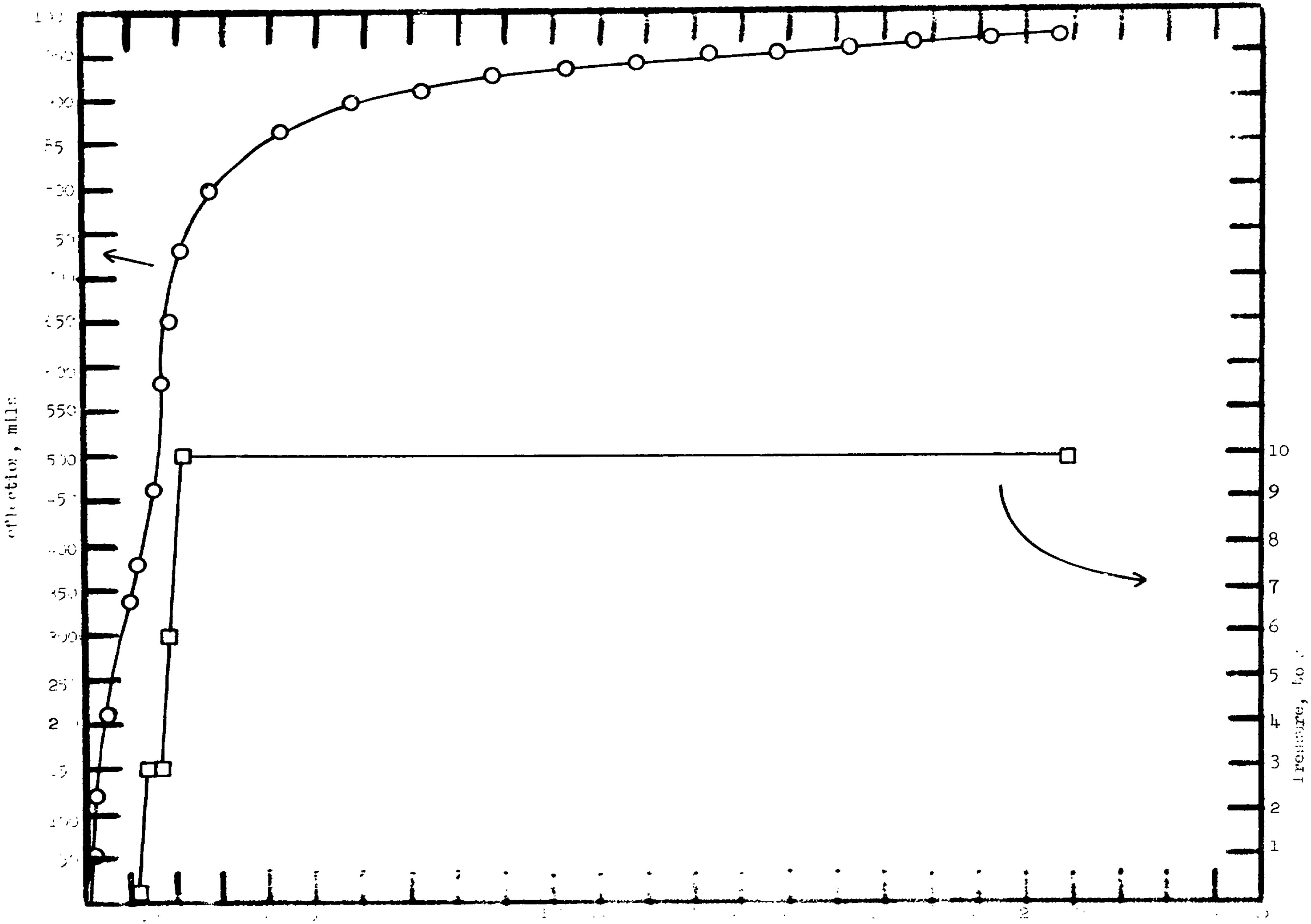

Figure 20. [illegible]eformation-Pressure-Time Plot for [illegible]

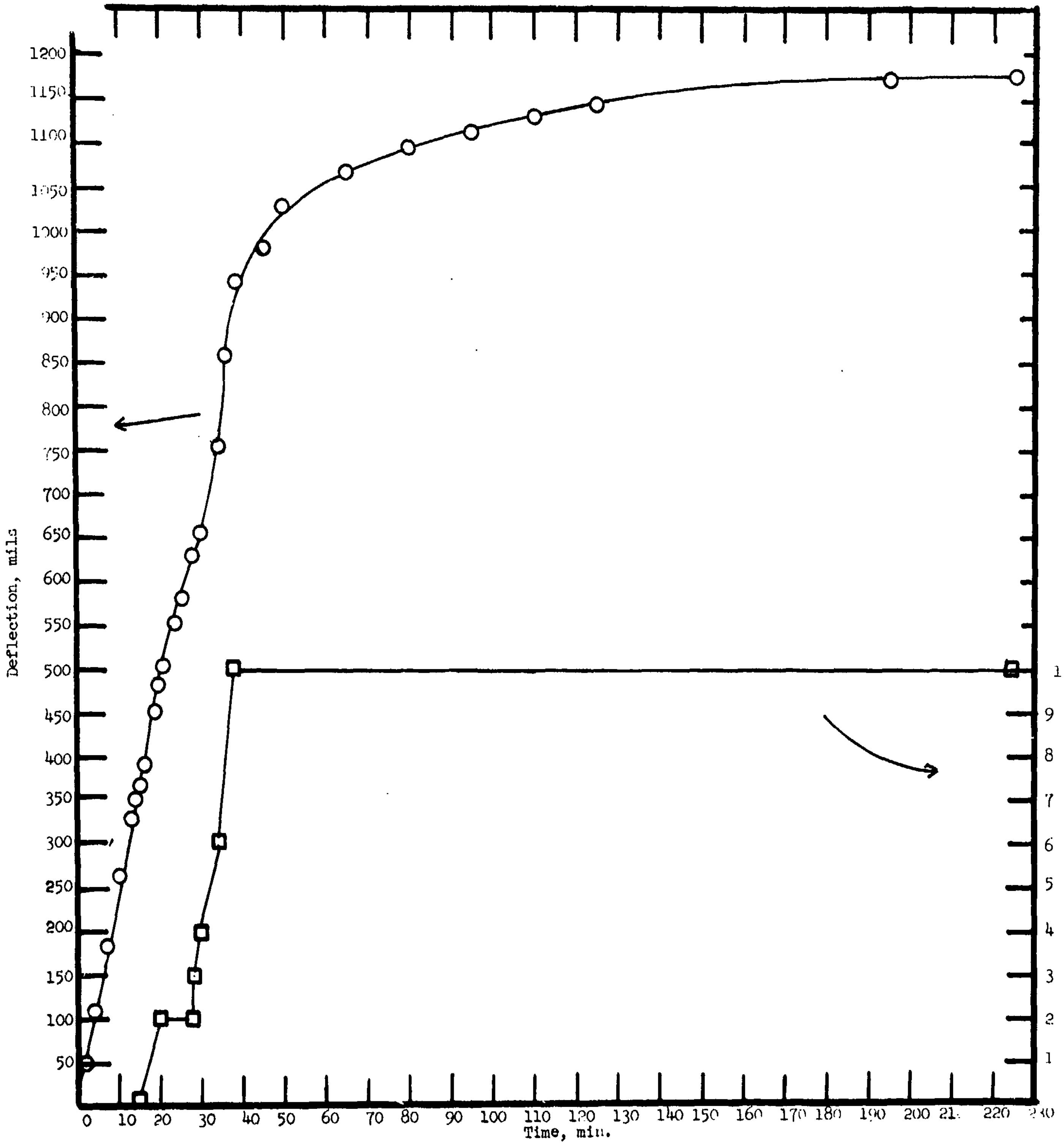

Figure 21. Deformation-Pressure-Time Plot for Forging 1670.

direction probably caused the poor densification, and no further similar runs were conducted.

Run 1722 was conducted under the reduced strain rate conditions of 1675 with intermediate holds at 4 and 6 tons. The total time under pressure was reduced from 225 minutes to 180 minutes. The results, however, were quite similar in that a 75% depth of forging was achieved. Edge tears were somewhat reduced over 1675, but they were not reduced to the point where it was worth the penalty in reduced depth of forging. This forging also suffered from a defect not previously observed in forged hemispheres; the concave surface was covered with black spherical defects. The particular lot of Vendor I powder used has shown spherical shade zone defects. An optical inspection of these defects led to the conclusion that they could be caused by either contamination from the BN lubricant or the Al_2O_3 powder.

The MgO doping level was reduced from 0.2 to 0.12% for run 1727 as $MgAl_2O_4$ had been identified by x-ray diffraction on forging 1493[14] and 1576 which contained 0.2% MgO. Although the reduced strain rate forging conditions were employed, a large sudden deflection was noted during the run, and the resultant piece showed a circumferential crack. The depth of forging was 58% indicating high friction and resistance to forging. This was probably due to the cracking early in the forging. The partial hemisphere was quite translucent especially considering the 0.2 inch wall thickness. The cracking may have been due to grain growth from the reduced MgO concentration, but further runs are necessary to establish whether or not this is a problem.

F. Characterization of Forged Hemispheres

Microstructural analysis of 1576 revealed an extremely dense 20 um grain intercept structure as illustrated in Figure 22. Approximately 5 v/o $MgAl_2O_4$ second phase was observed which apparently results from the 0.2 w/o MgO addition. It was estimated from the x-ray lattice parameter (a_o = 7.95 Å) results for the spinel phase[17] that the composition was 81 w/o Al_2O_3. This is within the solid solution spinel field at the forging temperature. At this composition each Mg^{+2} ion over solid solubility has considerable leverage as it brings 8 Al^{+3} and 13 O^{-2} with it into the spinel field. The edge of the specimen was free of spinel phase, suggesting that Mg^{+2} had volatilized from the surface. Analogous results are observed for the same reason.

Figure 23 illustrates the microstructure of forging 1727. This forging was more porous than 1576 as expected from the incomplete forging. It was interesting that the spinel phase was observed with only 0.12 w/o MgO additive. The spinel concentration was estimated at 3 v/o based on a lineal analysis.

X-ray analysis was conducted on forging 1576 for a determination of the presence and degree of orientation. A 3/8" square whose center was 13/16 from the apex was cut from the hemisphere. The convex side was ground flat so that the final surface was parallel to the plane tangent at its center. The orientation analysis was conducted according to the techniques discussed in Section D. An average of two x-ray scans for the two techniques

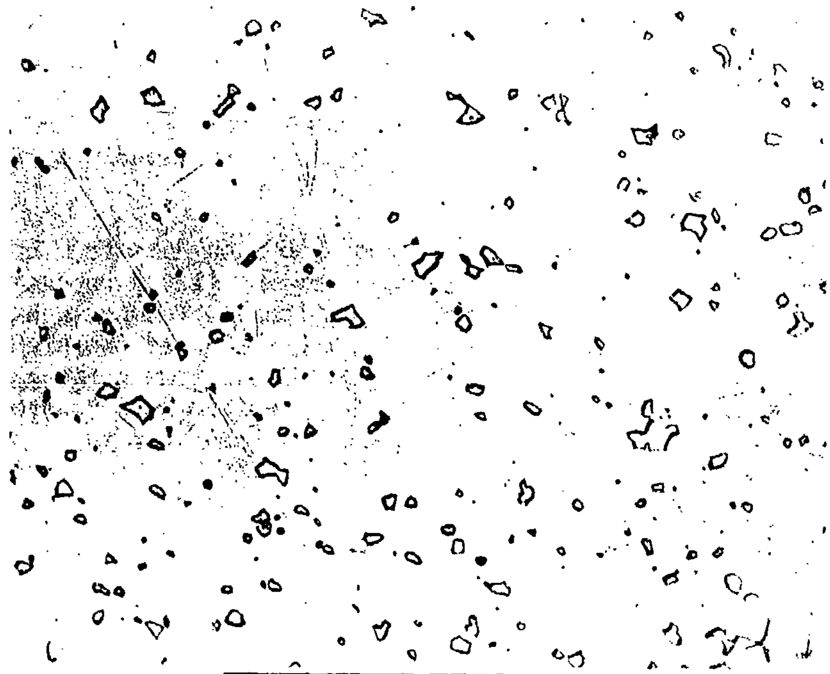

5598-2 250X

Figure 22. Relief Polished Cross Section of Hemisphere Forging 1576 with 0.2 w/o MgO Additive.

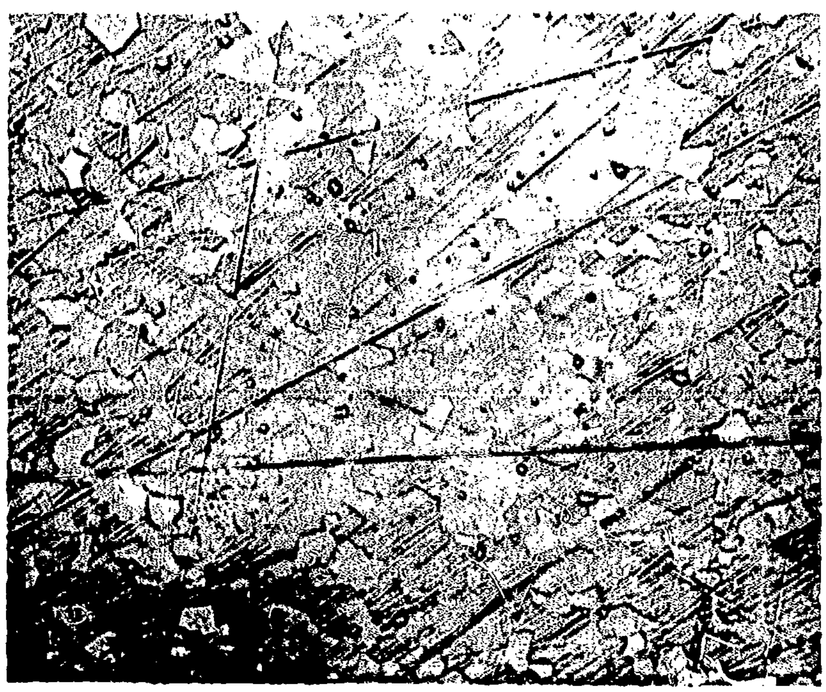

5597-2 250X

Figure 23. Relief Polished Cross Section of Hemisphere Forging 1727 with 0.12 w/o MgO Additive.

were calculated and is shown in Figure 24. An unoriented sample would indicate a straight line at R = 1 for both R_1 and R_2. The shape of the curve is identical for both analyses confirming the predictions and revealing a high degree of orientation in the forged hemisphere. The new method of data reduction appears feasible and should prove valuable in future texture analyses of forged samples.

The 1576 orientation data is compared with data from hemisphere 1432 produced last year[14g] and a flat disc forging (1277) produced earlier[14e] in Figure 25. All data was taken for a position within one inch of the center of each forging. The flat disc forging exhibited the highest degree of near center orientation achieved to date. The recent forging shows a 65% improvement in orientation over the early hemisphere. However, the orientation is 50% of that achieved for the best disc forging. A rim section of disc forging 1151[14f] showed $R_{\phi=0}$=51, which is the strongest basal orientation yet observed.

The section of hemisphere 1576 used for the orientation study was polished and is shown in Figure 26. The total and in-line transmission was measured with a Beckman DK2 Spectrophotometer from 0.5 to 2.5 wavelength and is plotted in Figure 27. Also shown is in-line transmission data between 2.5 - 7.5 microns wavelength collected both for the 1576 flat square and hemisphere 1577 with a Perkin Elmer 621 Spectrophotometer. Transmission for the 1577 hemisphere (pictured in Figure 18) was taken through the apex which corresponds to the dead zone in the forging. Transmission for other positions could not be measured due to fixturing problems, but qualitatively, the transparency was slightly poorer in the center than the side wall. The hemisphere wall thickness was approximately three times the thickness of the 1576 square, thus the higher transmission for the latter sample was expected.

Two press forged Al_2O_3 specimens were tested in the Avco ten megawatt arc facility. For comparative purposes, two $MgAl_2O_4$ specimens produced on another program[18] were also tested. The 2 x 2 x 0.25 inch specimens were mounted on a 2 x 7.5 x 0.260 inch Al backplate and bonded with an ablative epoxy which covered the remaining portion of the backplate. The inserts were placed in a water cooled wedge located in a 10 MW arc heated supersonic air stream. The test conditions are reported in Table VI. All specimens survived the thermal shock environment with no cracking. It was especially noteworthy that 1188 Al_2O_3 specimen survived a mechanical shock as well as a thermal shock as it was blown considerably downstream when it became unbonded.

One press forged Al_2O_3 and one $MgAl_2O_4$ circular right cylinder specimen were tested for rain erosion resistance in the Avco rain erosion test facility at a nominal encounter speed of 4000 ft/sec through a 40 ft rain field with a water concentration of 0.674 gm/m^3. A 90° encounter angle was employed. The data is reported in Table VII. The mass loss ratio is the mass of sample lost during flight over the mass of H_2O encountered during flight. Both sp imens developed surface cracks and considerable loss although the $MgAl_2O_4$ was about 5 times worse. This difference in resistance is accentuated due to the erosion of entire chips in the $MgAl_2O_4$ specimen.

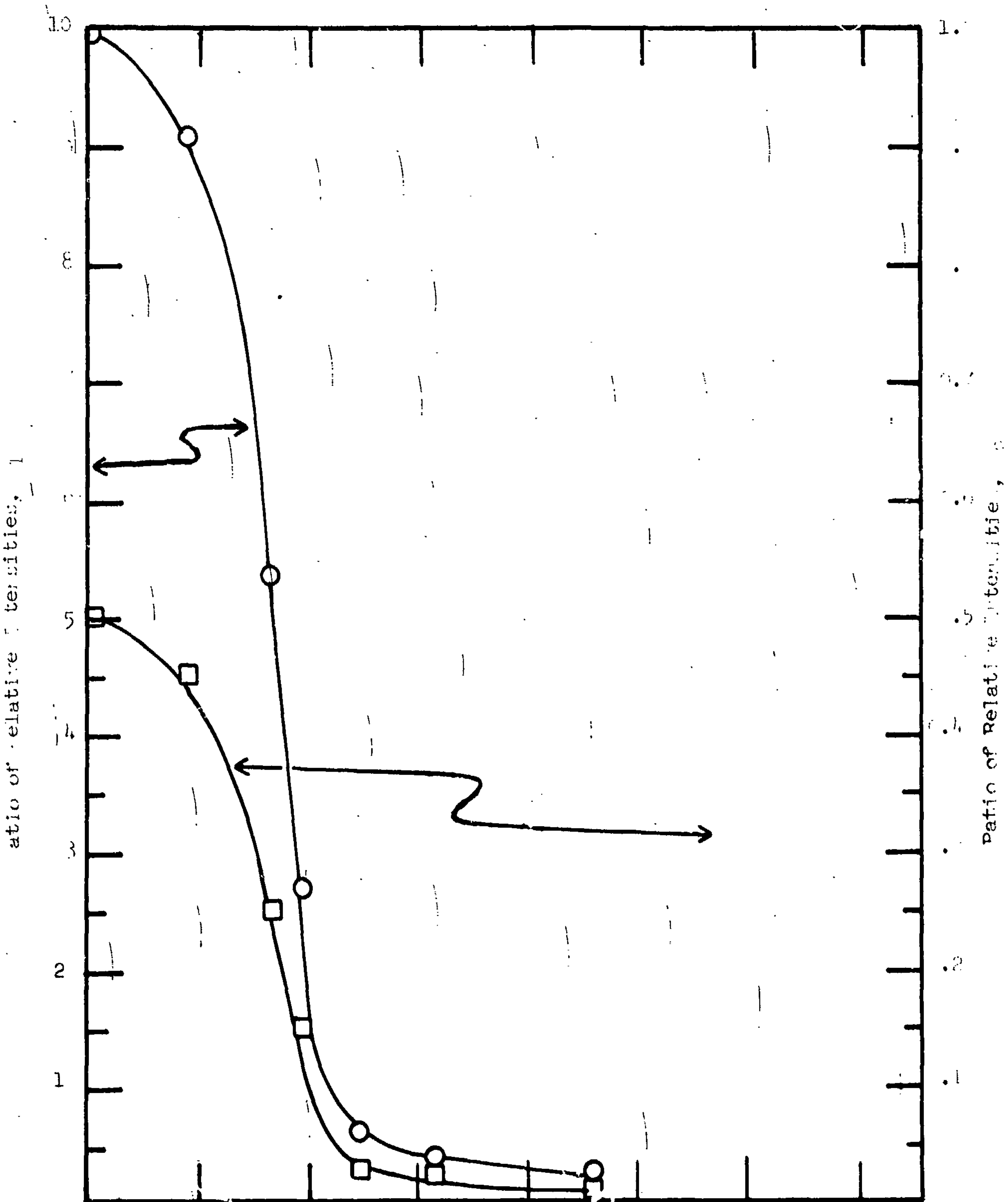

Figure 2?. 'atio of 'elative X-ray Intensity alculated two Ways for Forged hemisphere 15?6 Versus Powder as a Function of Angle from Basal Plane.

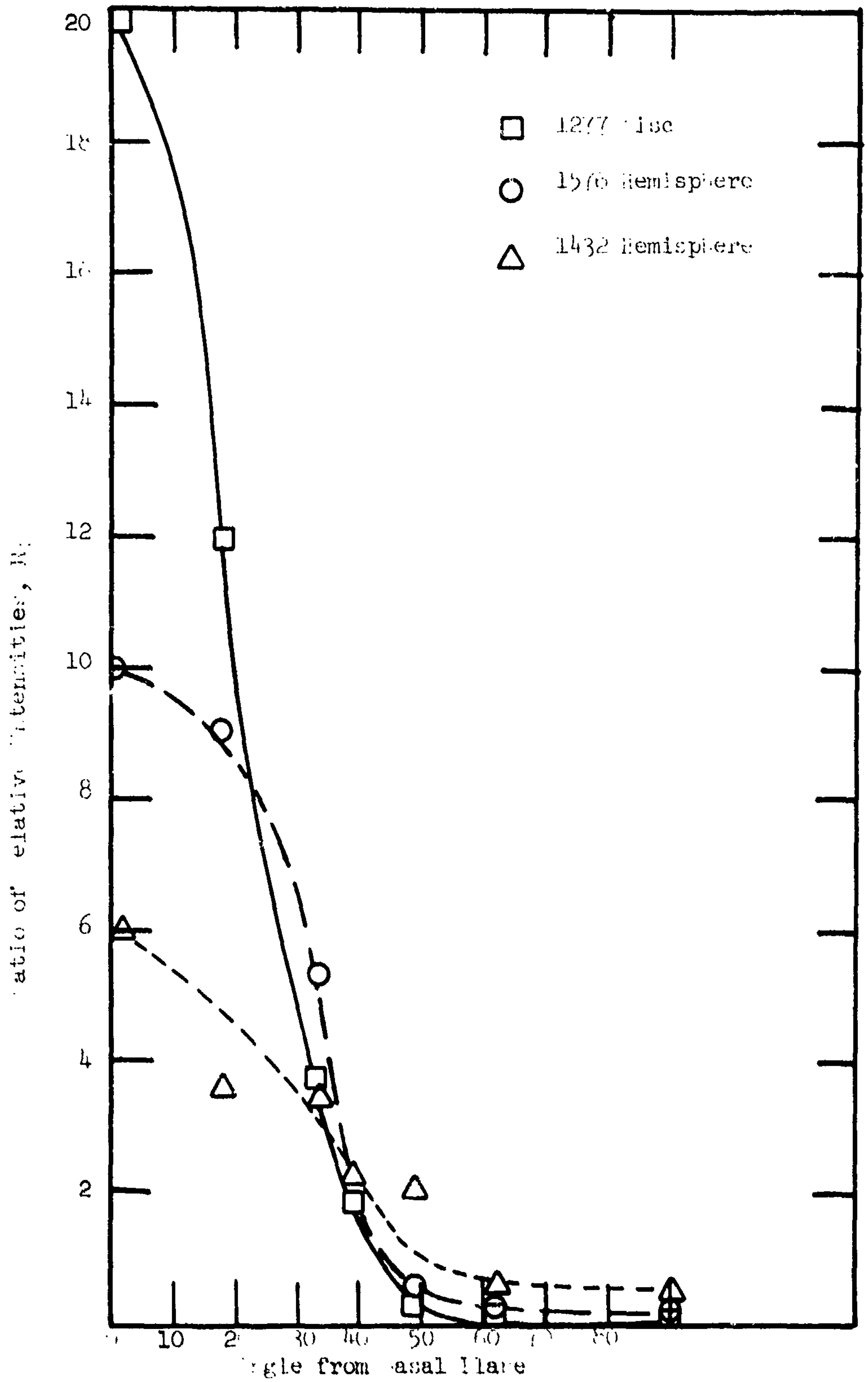

Figure 25. Ratio of relative x-ray intensity for several forged Al_2O_3 samples versus powder as a function of angle from basal plane.

AVCO CORPORATION

Figure 26. Polished Section of Hemispherical Forging 1576.

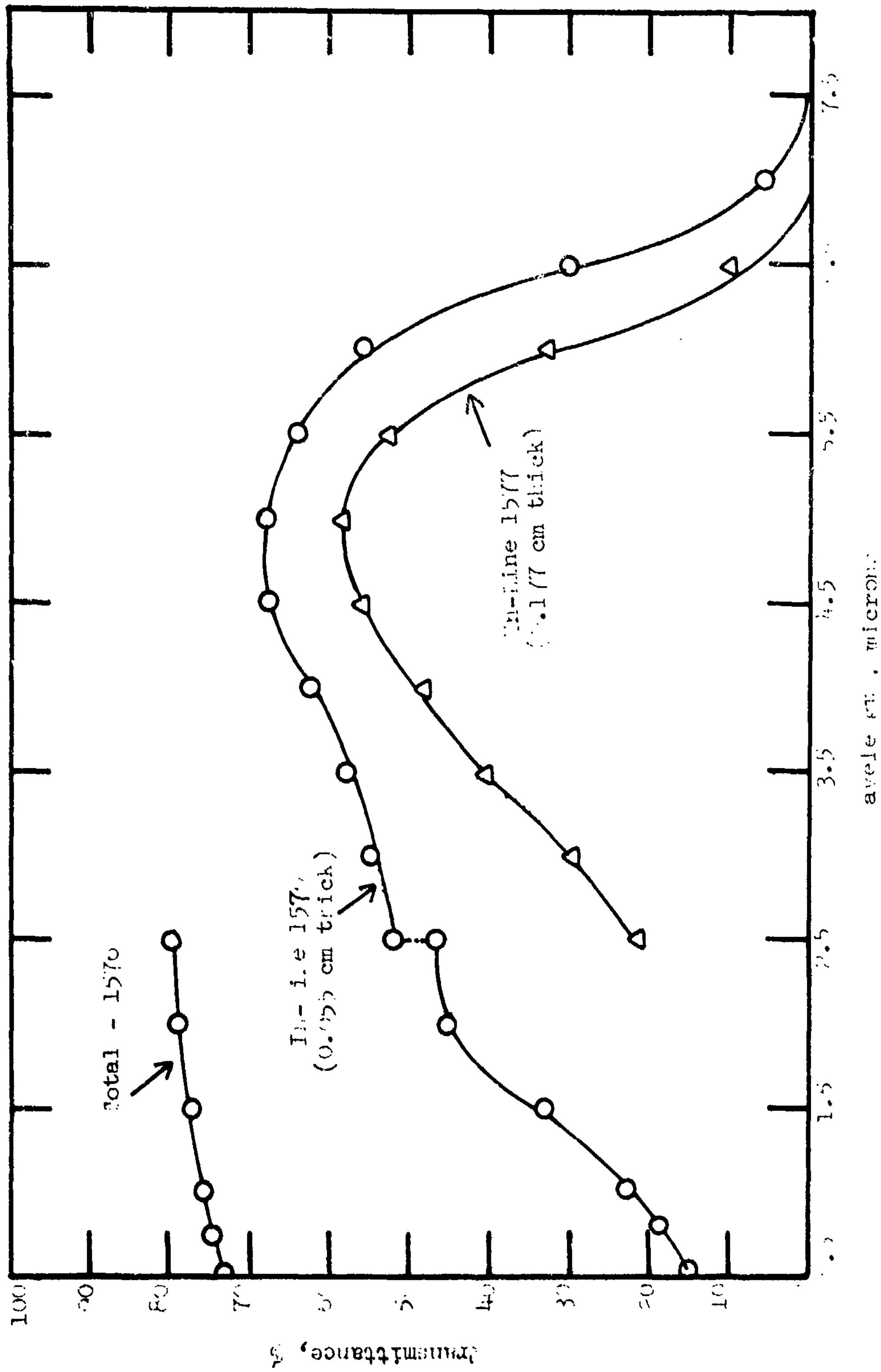

Figure 27. Transmission versus wavelength for a section of Hemisphere 1576 and full Hemisphere 1577.

Table VI

10 MW Arc Test Summary

Run No.	Specimen No.	Material	Gas Enthalpy Btu/lb	Cold Wall Heat Flux Btu/ft^2-sec	Shear lb/ft^2	Test Time Seconds	Peak Surface Brightness Temp. °C	Remarks
9448	D1188	Al_2O_4	657	76	11.4	12.83	1811	Run cut, specimen blew out, no cracks.
9452	D1187	Al_2O_3	667	58	8.5	14.99	1625	Specimen sound.
9449	1406	$MgAl_2O_4$	657	76	11.4	10.00	1825	Specimen sound.
9453	1404	$MgAl_2O_4$	667	58	8.5	14.98	1545	Specimen sound.

Table VII

RAIN EROSION TEST SUMMARY

Specimen No.	Material	Test Velocity ft/sec	Mass Loss Ratio	Mean Mass Loss Ratio	Comments
1161	Al_2O_3	4550 4075 3990	0.48 0.28 0.43	0.40	Slight macroscopic cracks.
1399	$MgAl_2O_4$	4130	2.08	2.08	Severe macroscopic cracks observed and pieces of specimen were lost in flight or recovery.

G. Discussion

The hemispherical forging experiments centered on the following process variables; strain rate control, lubrication, preform geometry, and preform microstructure. The MgO doping level received minor attention. Forging temperature, pressure, and hold time were not varied during this experimental series.

Three runs exhibited circumferential cracks which apparently developed early in each run. The cracks developed because the imposed force produced a strain rate that exceeded the flow stress for the temperature and microstructure at that instant in the process. The exact conditions cannot be defined, but approximate "safe" forging conditions at 1880°C, 50-96% starting density are 0.050 inch/minute during the initial 10% reduction, 0.030 inch/minute during the next 75% reduction, and 0.020 inch/minute for the remainder of the cycle. Even with these conditions, fracturing may occur on occasion. Four good forgings were performed under these conditions achieving a very acceptable 92% depth of forging. It is thought that the above conditions describe an upper deflection rate for successful forging. However, it appears that lower strain rates also lead to problems. Runs 1675 and 1722 had deflection rates of 0.011 inch/minute after the first 10% reduction and as noted in Table V, incomplete forging occurred. This was probably due to the fact that flow stress is inversely proportional to grain size to some power function, and by slowing down the deformation process, grain growth occurs and the flow stress is raised above the imposed force. The force could be raised some increment, but the fracture stress of some of the graphite components is close to this level. As well as being a good strain rate to achieve full forging, edge tears appear to be minimized.

Variation of the lubrication technique demonstrated in a qualitative sense that the lubrication variable was important. The application of a thin undercoat layer of graphite paint over the male punch was desirable. Run 1603 included this undercoat on the female punch too, and a reduced depth of forging was achieved. This does not seem logical, thus in retrospect, the reduced depth of forging may have been due to other effects such as grain growth. All forgings employed a layer of BN on both punches. This appears helpful and necessary for good results. The grade and quality of the BN appears to be important. Some variability in results may have been related to shifting from one lot to another of the same grade BN. All of the BN employed was from one manufacturer*, and good results were obtained for both the HTP and the HPT grades.

A pre-sintered preform was employed for all forging and is preferred over a loose powder or cold pressed preforms used previously[14g]. The main advantage is that second phase inclusions (microcracks and density gradients) are minimized. Preforms from 50% to 96% dense were used, but due to the fact that other variables were simultaneously introduced, it was not possible to determine which condition was preferred. It can be concluded that both 50% and 96% dense preforms resulted in very good and apparently equivalent final porosity forged hemispheres (1576 and 1577). Also a 50% dense starting preform must sinter to > 90% by the time forging is started. It is thought that as forging conditions are further narrowed, the higher density preform will be preferred because the pores will be closed and filled

*Carborundum Co.

with soluble H_2.

Most forging preforms were 1 inch diameter by 1 inch high circular right solid cylinders with a hemispherical cap. Although good forgings were achieved with this geometry, it is thought that the straight right cylinder is preferred because for this geometry, the apex receives greater deformation. This has the potential effect of improving the transparency of the region normally considered to be a dead zone. The experiments performed to date do not definitively answer this question. The preform for 1576 was shaped to fit 120° arc of the die. Although the total deformation was less for this geometry, very good results were achieved. The depth of the edge tears was considerably reduced for this geometry which is a big advantage. The crystallographic orientation for this specimen was better than previously achieved on a hemisphere, but it is expected that the right cylinder preform geometry would give an advantage in that regard.

Roy and Coble[6] estimated that 0.11 w/o MgO would be soluble in Al_2O_3 at 1830°C in vacuum. Based on the 3 v/o spinel found in forging 1727 with a 0.12 w/o MgO starting composition (Figure 23), it appears that the solubility is considerably reduced in the CO-CO_2-A press forging atmosphere. The spinel phase must stabilize grain size contributing to the ease of forging and pore removal by diffusional processes. However, it is undoubtedly a contribution to the effective material's absorption of radiation. Thus, further work must be performed to either determine the correct concentration of MgO for forging or effect the dissolution of the spinel phase through heat treatment.

Previous discussion has dealt with the phenomenological development of crystallographic structures in Al_2O_3[14b]. Basal slip has the lowest yield stress in Al_2O_3, thus, as shear stresses and bending moments develop on each grain due to the imposed force, basal slip begins and as it proceeds, the grain rotates to become oriented with its basal plane normal to the imposed force. Not all grains participate in this process or orientation would be complete. Other deformation mechanisms such as diffusional creep, grain boundary sliding, and non-basal slip contribute to the total deformation. Considerable evidence has been obtained that primary recrystallization occurs during the forging process. Preferred nucleation apparently accounts for the fact that the crystallographic deformation structure is retained through the recrystallization process. The improved orientation for 1576 compared to the earlier hemisphere 1493 is a result of gradual refinement of the process. The 120° cap preform used in forging 1576 would be expected to require less deformation (less orientation) than the right cylinder preform used in 1493. Even though the orientating was not as great as has been observed, many disc forgings have exhibited $R_{\phi=0} \sim 10$.

In-line transmission was in the 40-70% range for the infrared wavelength region. The greater transmissivity for a square sectioned from hemisphere 1576 compared with the apex region of hemisphere 1577 was due to a reduced thickness for the former sample. The hemisphere had some visually apparent porosity in the region where the measurement was made compared with the side wall; thus, the maximum transmissivity could be expected to be some increment higher.

The infrared transmissivities of the hemisphere forgings are compared with earlier flat disc forging in Figure 28. When transmission loss for increasing thickness is considered, forging 1576 actually shows up slightly inferior to 1577. Both hemispheres appear better than disc forging 110, but not quite as good as disc forgings 103 and 47. Besides true material absorption, the transmission loss is attributed to grain boundary scattering, phase boundary scattering, porosity, impurities, and other imperfections. The disc forgings were pure Al_2O_3; thus they were free of $MgAl_2O_4$ phase, which probably accounts for their slightly high transmissivities. It is obvious that the other factors listed are important since two sections of 110 disc forging had lower transmissivities than the hemispheres. The fact that the hemispheres exhibited optical properties so close to the disc forging lends considerable encouragement toward achieving the overall good of this task; forging shapes with the optimum properties of press forged Al_2O_3.

The arc testing demonstrated that both press forged Al_2O_3 and $MgAl_2O_4$ possess enough thermal shock resistance to survive a moderate tactical missile aerodynamic heating environment. The environment was not sufficiently severe to separate which material was superior, although Al_2O_3 is usually considered to have better thermal stress resistance.

The rain erosion testing was at a very high velocity for some applications, but it was clear that Al_2O_3 was far better than $MgAl_2O_4$. This was expected because of the known reactivity of MgO and H_2O. The Mg:O bonds in $MgAl_2O_4$ are expected to be almost as susceptible to attack as in pure MgO. Also, strength is an important criteria in erosion resistance[19] and the Al_2O_3 was $\sim$ 30 Kpsi stronger than $MgAl_2O_4$[18].

H. Conclusions

1. Complete alumina hemispheres with high in-line transmission have been press forged from pre-sintered preforms. Further improvements are possible, but properties near those of the best disc forgings were achieved.

2. A preferred basal crystallographic texture was developed parallel to the hemisphere surface which was attributed to basal slip playing a strong role in the deformation process. Improved orientation for a hemisphere was achieved in this program, but the results do not yet match the strongest orientation in disc forgings.

3. Deformation rate control is very critical as high rates crack the forging and low rates result in incomplete forgings. A deformation rate schedule was mapped out and resulted in four successful hemispheres. Two of these hemispheres subsequently developed cracks due to punch sticking problems during cool down.

4. Lubrication in the form of BN cover coat over graphite paint is beneficial to the forging process.

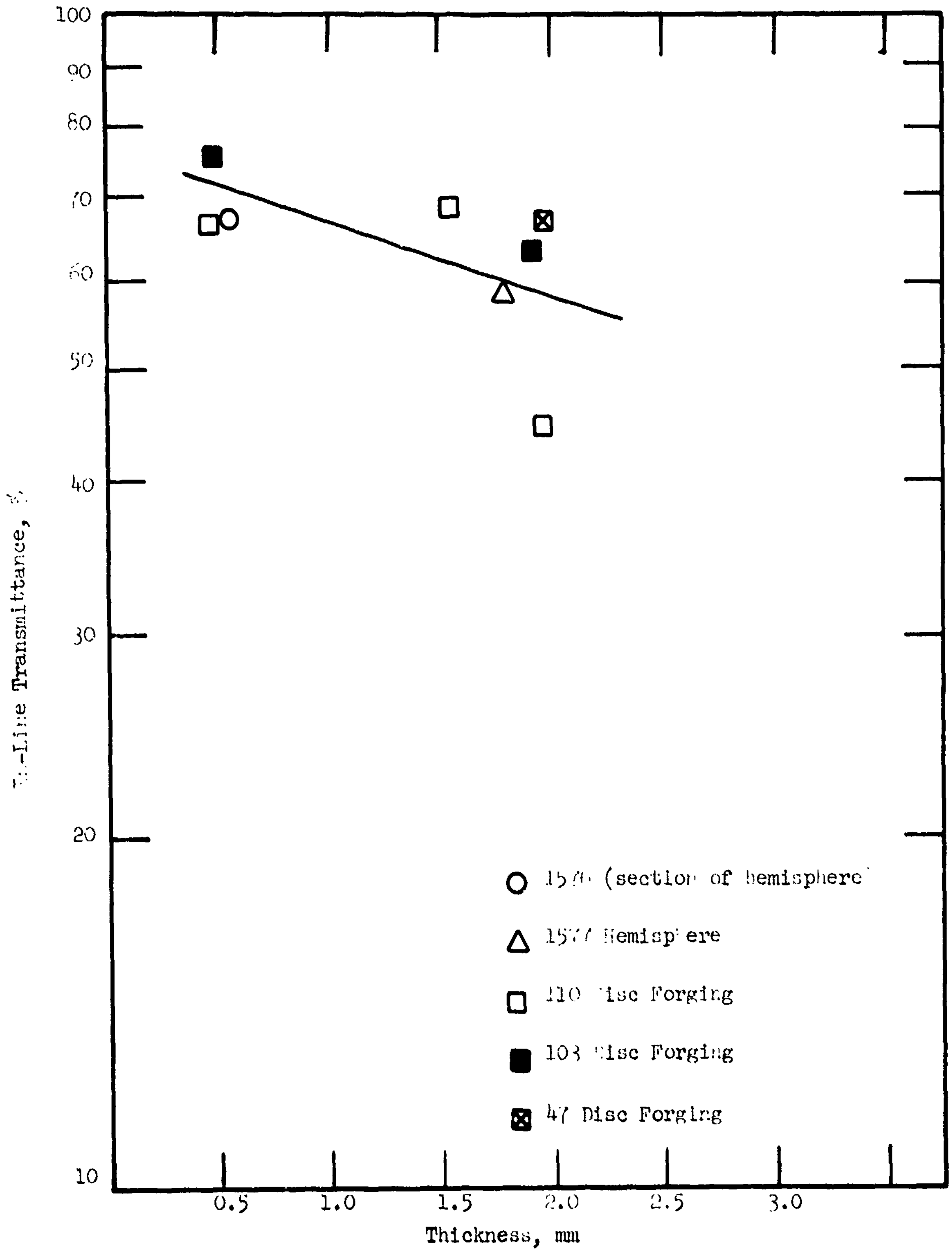

Figure 28. Transmittance of Hemispheres Compared with Disc Forgings versus Thickness at 5 μm Wavelength.

5. Sintered preforms are preferred over cold pressed preforms used in previous efforts, and the circular right cylinder geometry appears satisfactory although other geometries such as a partial hemisphere show promise.

6. Transmissivity for two forged hemispheres was only slightly lower at 5 µm than the best flat disc forgings. This was probably due to the free spinel phase in the disc forgings.

7. Arc testing in a moderate aerodynamic environment showed press forged Al_2O_3 and $MgAl_2O_4$ to possess adequate thermal shock resistance to survive.

8. The rain erosion resistance at 4000 ft/sec of press forged Al_2O_3 is superior to press forged $MgAl_2O_4$, probably due to the attack of the H_2O on the Mg:O bond, and the greater strength of Al_2O_3.

IV. HIGH PURITY Al_2O_3

A. General

This program has, for several years, dealt with the preparation and properties of high purity Al_2O_3. The main reason for this involvement was the lack of sufficiently pure polycrystalline Al_2O_3 for property studies. This made it impossible to distinguish between structure-sensitive and composition-sensitive mechanical behavior. The discussion in Section II was indicative of the complicating effects of impurities on brittle mechanical properties. Recently[14g], a deformation study on one grade of hot pressed high purity polycrystalline Al_2O_3 containing 300 ppm anion and cation impurities (mass spectrometric analysis) contributed significantly to increased understanding of the deformation process.

Mr. K.S. Mazdiyasni of the Wright-Patterson Air Force Materials Laboratory has long been interested in producing high purity oxide powders from organo-metallics. High purity fine particulate yttria-stabilized zirconia was produced in sizable quantities, and one of the authors was involved in a detailed processing study on this material[20]. Recently, Mr. Mazdiyasni has produced Al_2O_3 with approximately 30 ppm cation impurities; thus, it was decided to participate in a cooperative program with AFML aimed toward the fabrication of high purity polycrystalline Al_2O_3 from an organo-metallic synthesis route. It was expected that ultimately some mechanical or other physical properties of these samples would be measured.

B. Powder

Preliminary work on the preparation of high purity Al_2O_3 from organo-metallics established that the dried hydrolized material was $5Al_2O_3 \cdot H_2O$ with about a 20 Å particle size as determined by electron shadowgraph techniques. Calcining the powder for 24 hours at 750°C increased the crystallite size to 100 Å and produced eta Al_2O_3. Conversion to alpha

Al_2O_3 occurred after a 1200°C calcination.

Preliminary lots 1-4 had an impurity analysis as shown in Table VIII. This was a semi-quantitative emission spectroscopy impurity analysis using 99.9999% Al reference material.

Several hundred grams of 99.9999% Al were supplied to AFML for conversion to Al_2O_3. This material was calcined by several techniques known to affect the agglomerate structure. The list of powder batches and their calcining conditions is given in Table IX.

C. Hot Pressing Results

Vacuum hot pressing was conducted in a resistance heated furnace using Poco high strength graphite dies. Considerable care was exercised in die cleaning and powder transfer operations. For example, the latter operations were conducted within a glove box. The hot pressing conditions and results are listed in Table X.

The initial set of hot pressing parameters was selected based on fabrication studies of high purity Al_2O_3 derived from recrystallized $Al_2(SO_4)_3$.[14f] Only 96.4% of theoretical density was obtained for run 1578, using powder calcined at 1150°C where a density in excess of 99.5% was expected. The next five pressings were conducted using the same powder lot in an effort to achieve the desired density. First the time parameter was increased from 10 to 60 minutes with a resulting improvement to 99.1% density. Then temperature was increased from 1400°C to 1450°C and finally 1500°C. The density gain was marginal and judged not worth the increased grain size. Next, powders calcined at two lower temperatures (750° and 950°C) were pressed under modified conditions based on the initial series with resultant densities of only 92 and 97.2% of theoretical.

Observations during a sintering study on the organometallic derived Zyttrite powder led to the conclusion that the agglomerate structure affected both the kinetics and microstructure development during consolidation[20]. Water washed Zyttrite resulted in plate-like pore pockets. Alcohol washing of Zyttrite powders during the last stages of the powder process reduced the interagglomerate crystallite bonding to the point where, in the final powder compact, preferential interagglomerate sintering did not dominate the microstructure development. Various kinetic and microstructural observations led to the conclusion that intra-agglomerate sintering controlled the kinetics in the final stage of sintering. The water washed Zyttrite powders gave higher hot pressed density and did not show the unusual pore pockets noted in sintering. This reversal in kinetic behavior was never explained.

A series of three hot pressings were conducted with alcohol washed Al_2O_3 under the premise that alteration of the agglomerate structure would improve the consolidation kinetics in an analogous manner to Zyttrite. Runs 1609 and 1610 were conducted with an argon atmosphere in heating to 1250°C followed by switching to vacuum for the remainder of the run. This procedure reduces the turbulence in the chamber and powder column during the initial consolidation period at the expense of efficient outgassing. Run 1618

TABLE VIII

Impurity Analysis of Alkoxy-Derived Al_2O_3 Lots 1-4

Cation	Concentration ppm
Zr	8
Si	6
Ti	5
Ni	4
Fe	3
Mg	2
Pb	1

TABLE IX

Alkoxy-Derived Al_2O_3 Powder Preparation and Calcining Condition

Number	Wash	Calcination
1	Water	50°C - 24 hrs.
2	Water	550°C - ½ hr.
3	Water	750°C - ½ hr.
4	Water	950°C - ½ hr.
5	Triple Alcohol	50°C -
6	Triple Alcohol	1000°C - ½ hr.
7	Water	1150°C - ½ hr.

TABLE X

Hot Pressing of Alkoxy-Derived Al_2O_3

Pressing Number	Powder Lot	Temp. °C	Pressure Kpsi	Time min.	Density % Theoretical
1578	7	1400	15	10	96.4
1588	7	1404	15	35	98.9
1589	7	1406	15	62	99.1
1590	7	1450	15	60	99.3
1591	7	1500	15	91	98.9
1593	7	1500	15	137	99.2
1594	3	1400	15	35	92.0
1595	4	1500	15	60	97.2
1609*	6	1400	15	35	95.1
1610*	6	1400	15	60	96.5
1618	6	1400	15	60	97.0
1620	7	1400	15	60	97.2

*Argon to 1250°, then vacuum.

was performed in vacuum atmosphere throughout and a slight gain in final density from 96.5 to 97.0% was noted.

The last run conducted during this program was a repeat of an earlier run with lot 7 powder. Since considerable time and a furnace rebuilding occurred between the early runs (1589 and 1620), it also served as a measure of reproducibility. The 97.2% relative density was 2.9% lower than achieved for 1589 indicating conditions were in some way altered compared with the early experiments. It is most likely that the sample temperature was lower than previously existed for the same observed temperature. Having run 1620 did make it possible to draw some conclusions for the various powder lots (Section E).

D. Characterization

A complete microstructural analysis was performed on sample 1589. Figure 29a illustrates the presence of about 1% porosity with a nonuniform distribution. Figure 29b is a fractograph showing considerable transgranular fracture and the beginning of exaggerated grain growth. The grain intercept was 3.1 μm. Figure 29c illustrates a pore pocket found on a fractured grain face.

The Knoop hardness of this specimen was 2090 kg/mm^2. The value agrees well with literature values for Al_2O_3.

E. Discussion

The organo-metallic route for Al_2O_3 powder synthesis appears capable of achieving a high purity fine particulate powder. The water washed powder exhibited microscopic evidence for tight well bonded agglomerates. The alcohol washed powder was not examined. The lot 7 water washed powder calcined at 1150°C - $\frac{1}{2}$ hour received the major emphasis. Although the crystallite size was not measured, it was thought to be $\ll$1000 Å. Based on a comparison of density achieved for a given process cycle with 3000 Å sulfate derived powder, powder lot 7 does not appear particularly active. Powder lots 3 and 4, which are close to 100 Å crystallite size, exhibited final densification kinetics even slower than lot 7. This, of course, does not fit kinetic models based on diffusional control of densification where densification rate is $\propto (\text{size})^{-3}$.

The microstructure study showed that very dense islands were separated by zones or pockets of somewhat higher porosity. Evidence was obtained for a pocket of pores on one grain face. The grain structure showed signs of exaggerated grain growth, although the 3.1 μm grain intercept was remarkably close to the 3.2 μm grain intercept achieved for the sulfate derived high purity Al_2O_3 processed by an identical cycle.[14g]

Combining these facts leads to the conclusion that interagglomerate sintering dominates the densification to the detrement of intra-agglomerate sintering. This explains the dense islands surrounded by porous zones. Apparently the between-agglomerate densification occurs in a sequential fashion after the interagglomerate sintering leading to the slow kinetics.

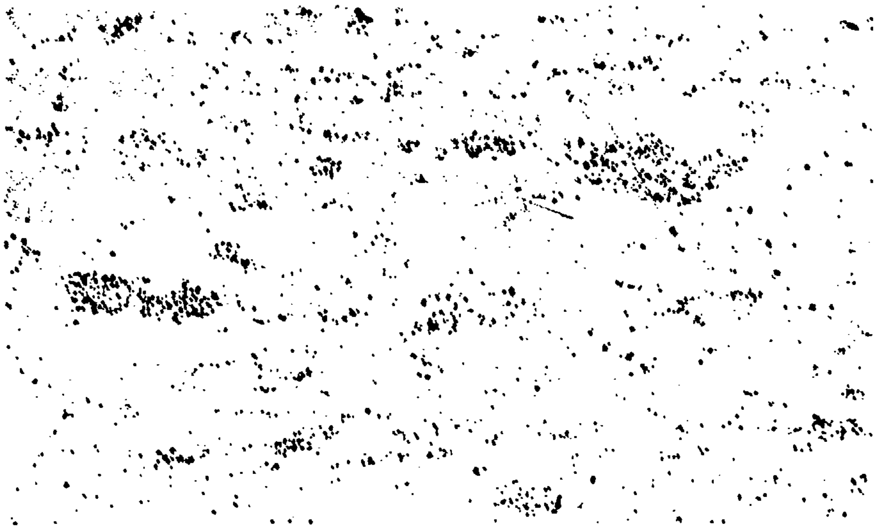

5458-1 (a) 100X

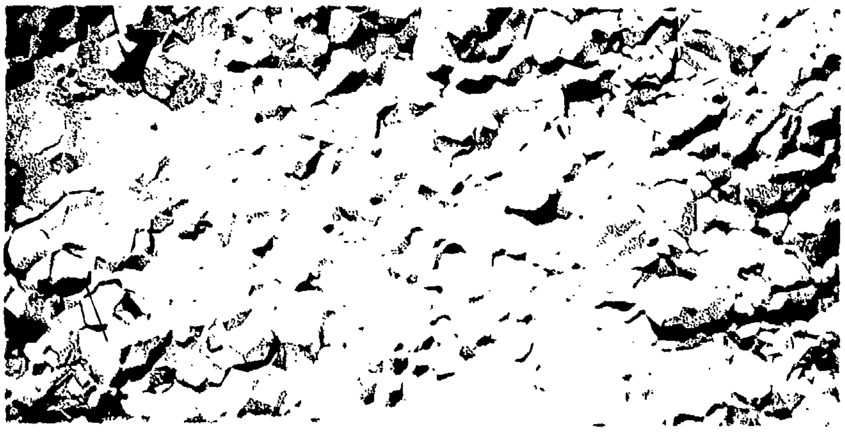

71162 (b) 1500X

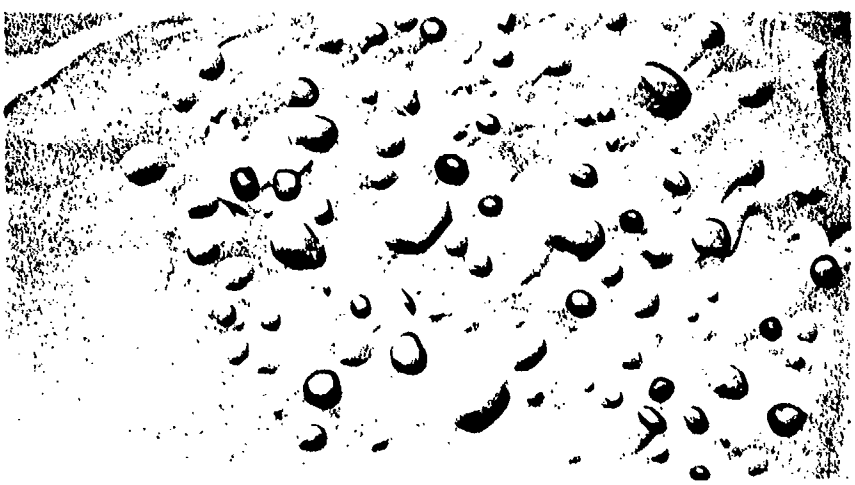

71165 (c) 30,000X

Figure 29. Microstructure of Alkoxy-Derived Al_2O_3 Hot Pressed to 99.1% Density.

The high concentration of pores, especially on grain faces, is unusual, and it is quite probable that a contributing factor to the pore concentration is gas entrapment. The high surface area powder could be expected to have a considerable volume of adsorbed gas. As this gas evolves, it would collect at the agglomerate boundaries which, according to the proposed model, undergo densification last.

The alcohol washed powder did not improve the consolidation kinetics. Neither the powder or consolidated microstructure have been critically examined, so conclusions cannot be made concerning the effectiveness of the alcohol washing on microstructure development. The effect of the alcohol wash on consolidation kinetics is exaggerated by the apparent alteration in thermal environment between the early runs and runs 1618 and 1620. The closeness in densities of the latter runs indicates that the kinetics are only slightly slower for the alcohol washed powder and further work with these powders appears justified pending microstructure examination.

F. Conclusions

1. The organo-metallic route for Al_2O_3 powder synthesis appears capable of achieving a high purity fine particulate powder.

2. The consolidation kinetics are slower than would be predicted for the fine particulate size. Based on this observation and porosity distribution in one 99.1% dense sample, it is concluded that interagglomerate densification is completed first. Both kinetics and final microstructure development are controlled by intra-agglomerate diffusional processes for water washed powder.

3. It remains uncertain whether or not alcohol washing is advantageous.

4. It remains uncertain whether or not a truly unique high purity, high density, fine grained Al_2O_3 can be achieved by hot pressing organometallic produced powder.

V. REFERENCES

1. C.D. Pears and H. Starrett, "An Experimental Study of the Weibull Volume Theory," AFML-TR-66-228.

2. T. Vasilos, private communication based on mass spectrometer analyses.

3. D.L. Vrooman and J.E. Ritter, Am. Ceram. Soc. Bull. 49, 789 (1970).

4. E.B. Shad, J. Am. Ceram. Soc., 48, 43 (1965).

5. H.P. Kirchner, W.R. Buessem, R.M. Gruver, D.R. Platts, R.E. Walker, "Chemical Strengthening of Ceramic Materials," Contract N00019-70-C-0418.

6. S.K. Roy and R.L. Coble, J. Am. Ceram. Soc., 51, 1 (1968).

7. R. Rice and P.F. Becher, "Effect of Surface Finishing on the Strength of Ceramics," Am. Ceram. Soc. Bull. 50, 374 (1971).

8. E.M. Passmore, R.M. Spriggs, and T. Vasilos, J. Am. Ceram. Soc. 48, 1 (1965).

9. R.J. Charles and R.R. Shaw, "Delayed Failure of Polycrystalline and Single Crystal Alumina," General Electric Report No. 62-RL-3081M.

10. R.M. Spriggs, J.B. Mitchell, and T. Vasilos, J. Am. Ceram. Soc., 47, 323 (1964).

11. R.W. Rice, Proc. Brit. Ceram. Soc., 12, 99 (1969).

12. a) Carniglia, S.C., J. Am. Ceram. Soc., 48, 580 (1965).
    b) Carniglia, S.C., Am. Ceram. Soc. Bull. 50, 184 (1971).

13. a) G.D. Swanson, "Fracture Energies of Ceramic Materials," Am. Ceram. Soc. Bull., 49, 390 (1970).
    b) L.A. Simpson, "Effect of Microstructure on Fracture Surface Energy Measurements of Alumina," Am. Ceram. Soc. Bull, 50, 784, (1971).

14. a) W.H. Rhodes, D.J. Sellers, A.H. Heuer and T. Vasilos, "Development and Evaluation of Transparent Aluminum Oxide," N178-8986, Final Report, (June 1967).
    b) A.H. Heuer, D.J. Sellers, and W.H. Rhodes, J. Am. Ceram. Soc., 9, 468 (1969).
    c) A.H. Heuer, W.H. Rhodes, D.J. Sellers and T. Vasilos, "Microstructure Studies of Polycrystalline Refractory Oxides," NOw-66-0506(d), Summary Report (1967).
    d) W.H. Rhodes, D.J. Sellers, R.M. Cannon, A.H. Heuer, W.R. Mitchell, and P.L. Burnett, "Microstructure Studies of Polycrystalline Refractory Oxides," Contract N00019-67-C-0336, Summary, 1968.

e) W.H. Rhodes, P.F. Jahn, P.L. Burnett, "Microstructure Studies of Refractory Polycrystalline Oxides," Contract N00019-68-C-0108, (June 1969).
f) W.H. Rhodes and R.M. Cannon, "Microstructure Studies of Refractory Polycrystalline Oxides," Contract N00019-69-C-0198, (December 1969).
g) W.H. Rhodes and R.M. Cannon, "Microstructure Studies of Refractory Polycrystalline Oxides," Contract N00019-70-C-0171.

15. R.L. Coble, J. Am. Ceram. Soc., 45, 123 (1962).

16. R.M. Haag, "Magnetic-Crystallographic Orientation Produced in Ferrites by Hot Working," Contract N00014-68-C-0364.

17. Roy, Roy, and Osborn, Am. J. Sci., 251, 337 (1953).

18. W.H. Rhodes, P.L. Berneburg, and J.E. Niesse, "Development of Transparent Spinel," Contract AMMRC-CR-70-19.

19. C.H. Bates and J.W. Morris, "Liquid Cavitation Damage to Single Crystal Sapphire," Symposium on the Science of Machining and Surface Finishing, National Bur. Stds., Nov. 4, 1970, Gaithersburg, Md.

20. W.H. Rhodes and R.M. Haag, "High Purity Fine Particulate Stabilized Zirconia (Zyttrite), AFML-TR-70-209.